ADDIS ABABA UNIVERSITY
SCHOOL OF GRADUATE STUDIES

MAPPING OF CRUSTAL THICKNESS VARIATION IN SOUTHERN AFAR USING GRAVITY SURVEY

BY

DESSALEGN TEKLE TIKU

ADDIS ABABA UNIVERSITY

JUNE, 2009.

ADDIS ABABA

MAPPING OF CRUSTAL THICKNESS VARIATION IN SOUTHERN AFAR USING GRAVITY SURVEY

BY

DESSALEGN TEKLE TIKU

A THESIS SUBMITTED TO THE SCHOOL OF GRADUATE STUDIES OF ADDIS ABABA

UNIVERSITY IN PARTIAL FULFILLMENT OF THE REQUIREMENTS FOR THE DEGREE OF

MASTERS OF SCIENCE IN EXPLORATION GEOPHYSICS

DEPARTMENT OF EARTH SCIENCES

ADDIS ABABA UNIVERSITY

JUNE, 2009

ADDIS ABABA

MAPPING OF CRUSTAL THICKNESS VARIATION IN SOUTHERN AFAR USING GRAVITY SURVEY

BY

DESSALEGN TEKLE TIKU

(DEPARTMENT OF EARTH SCIENCES)

APPROVED BY BOARD OF EXAMINERS

Dr. Tilahun Mammo _____

Advisor

Dr. Tigistu Haile _____

Examiner

Ato Befekadu Oluma _____

Ext. Examiner

ACKNOWLEDGMENTS

My heartfelt thanks go to my Advisor, Dr. Tilahun Mammo for the restless and invaluable academic advice that he gave me throughout this work. During this Thesis work, he has been my father, colleague and friend. There was no restriction of time to ask for help. Days and nights have been a time of work for us.

I am Grateful to my friends: Teketay Tsigie, Taddese Messelu, Mebatsion shawel, Aklilu Getachew, Abdisa, Elias, and Biruk Bereda for their helps, cooperation and encouragement.

Words of thanks should go to my families, particularly to my mother, Tsehynesh Ayalew and my father, Tekle Tiku for they gave me what I have.

I would like to say thank you for, Dr. Tigistu Haile, Dr. Abera Alemu, Ato Alemayehu and for all, who taught me.

I couldn`t forget the support from my former teachers, Ato Natniel Bimrew, Ato Gizachew, Ato Guadie, Ato Tesfahun, Muluken and Melsew.

Thanks should also go to all members in the Geophysics Department of the Faculty of Science, AAU.

Finally, I would like to thank Abdu Mohammed, Simachew Endale, Zemenu Temesgen, Mequanint Minuye, Muluken Belew, Getachew Yazie and Tefelga Tekle for their support and encouragement.

Dessalegn Tekle

TABLE OF CONTENTS

PAGES

List of Figures Pages

List of tables

ABSTRACT

The Afar Depression in north eastern Ethiopia is a scientific treasure trove. It is a site of a triple junction, where three plates (the Nubian plate, the Arabian plate, and the Somalian plate) are simultaneously pulling away from each other. The powerful stresses in the crust lead to frequent earth quakes and volcanism thereby producing deep cracks and fissures in the region. These tectonic activities and the sedimentation that occurs in the area change the topography, which affects the crustal thickness.

Analysis of the gravity data, obtained from the Ethiopian institute of geological survey (EIGS), constrained with seismic refraction results in the study area and the Euler deconvolution results produced here, was done to study the crustal thickness variation in the southern Afar Depression including the region between 8.8^0 to 11^0N and 39.8^0 to 42.7^0E . The Bouguer gravity, which shows the depression clearly separated from the rest of the study region by relatively higher values, is dominated by a strong regional gravity while the residual anomaly indicates elongated higher (positive) gravity values that follows a trend, which over laps with crustal extension (thinning) revealed by seismic refraction survey conducted in the area. Upward continuation results also support the idea that deeper effects influence the Bouguer gravity. Higher total horizontal gradient shows faulted structures. Particularly, this high gradient bounds the depression in the west and south east, which overlaps with the escarpment faults separating the depression from the western and south eastern plateaus. Gravity modeling using seismic refraction model and Euler deconvolution result, produced here, as constraints indicate a minimum crustal thickness of about 22.7 and 23.5 under profiles BB` and CC` respectively. The modeling also shows deep seated faults particularly under profile CC.

CHAPTER ONE

INTRODUCTION

1.1. Location

The Afar Depression is triangular in shape and is located at the separation zones of the Nubian, Somalian and Arabian plates. It constitutes a triple junction where the three major rifts, namely, the Main Ethiopian Rift, the Red Sea Rift and the Gulf of Aden Rift converge. It is considered to be the only emerged triple junction in the world (McKenzie and Morgan, 1969). This tectonically active triangular depression is bounded between 10^0 to 15^0N and 40^0 to 43^0E coordinates. It lies between the Red Sea and the Western and Eastern Ethiopian plateaus. This study focuses on the region between 8.8^0 to 11.9^0N and 39.8^0 to 42.7^0E. The rectangle in red color shows the study region (Figure1.1).

1.2. Back Ground of the Study

The unique geological situation of the Afar has intrigued earth scientists for a number of years. Not only is it situated between the East African Rifts, Gulf of Aden and the Red Sea but within it volcanic processes similar to those which take place at the inception of a spreading center might be observed at the surface. The triangular shape Afar depression is separated from the elevated areas of the Ethiopian plateau to the west, the Southeast plateau and Ogaden to the South and the Danakil Horst to the East by fault controlled escarpments. At the Southwestern apex of the triangle the east African Rift joins the depression. A series of active volcanoes exists in the Depression, providing spectacular out bursts from time to time. The Afar triple junction is a diffused extensional province where the Gulf of Aden, the Red Sea and the Main Ethiopian Rifts meet. The three rifts are different in age (Barberi et al., 1972; Cochran, 1981; Manighetti et al, 1998; Wolfenden et al., 2004) and spreading rate (Chu and Gordon, 1998; Bilham et al., 1999) but all tend to extend oblique to the corresponding rift axis (Joffe and Garfunkel, 1978; Boccaleti et al., 1994, 1998; Dauteuil et al., 2001; Huchon and Khanbari, 2003).

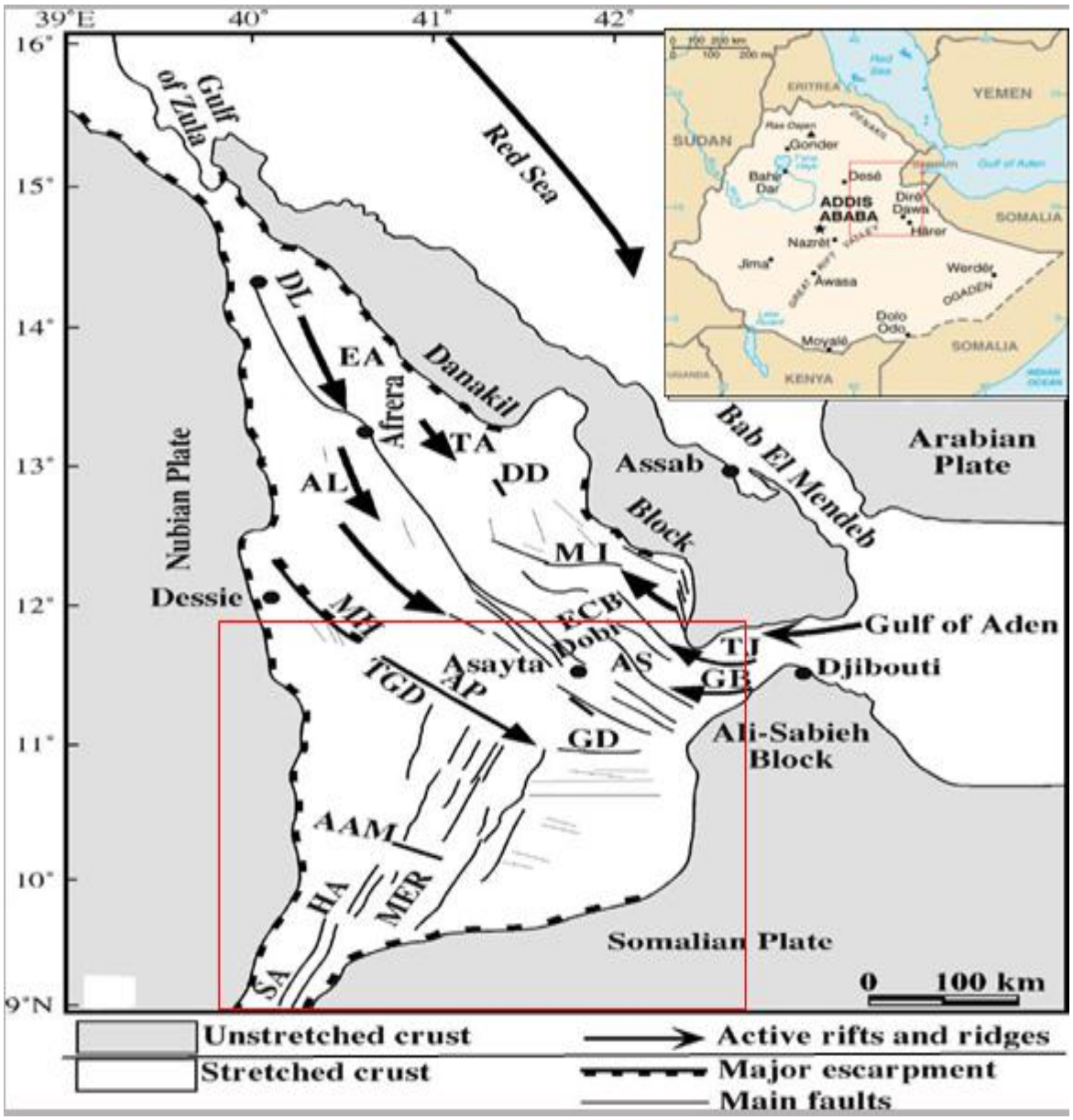

Figure1.1. (A) shows the location of the Afar Depression within NE Africa. (B) Tectonic map of the Afar Depression (after Manighetti et al., 1998, 2001). AAM = Ayelu Amoissa zone; AL = Alayata volcano; AP = Awsa plain; AS = Asal rift; DD = Dadar graben; DL = Dallol volcano; ECB = East-Central Block; EA = Erta Ale volcano; GB = Ghoubbet rift; HA = Herta Ale volcano; GD = Gobaad rift; TA = Tat Ale volcano; MER = Main Ethiopian Rift; MH =Manda Hararo rift; MI =Manda Inakir rift; SA = Sabure rift; TGD = Tendaho–Gobaad Discontinuity; TJ = Gulf of Tajura (modified from Beyene and Abdelsalam, 2005).

Several studies show that the Red Sea and the Gulf of Aden oceanic rifts are encroaching on land towards Afar (e.g. Courtillot, 1980, 1982; Acton and Stein, 1991; Manighetti et al., 1997, 1998, 2001; Figure1.1) as a result of the separation of Arabia from Africa and spreading didn't occur through the Bab El Mandeb Straight in recent times (Barberi et al., 1975) (Figure1.1). The rheology of the lithosphere beneath the Afar depression is weakened by one or more mantle plumes (Ebinger and Sleep, 1998; White et al., 1989) though the origin of the plume is still in controversy.

This jump of the Red sea and gulf of Aden rifts into Afar is in good agreement with the hypotheses that if rifting occurs close to the boundary between continental and oceanic crust, the rift would preferentially form on continental crust because of its rheological weakness (Vink et al., 1984;Müller et al., 2001). The interaction of three oblique rifts in a plume-affected lithosphere resulted into complex tectonics in Afar, making deformation so distributed that rigid plate kinematics doesn't apply currently in the interior of Afar. The Red Sea and Gulf of Aden rifts didn't connected directly so far and both have penetrated into Afar where they are now actively opening and propagating through the development of a series of disconnected, propagating rift segments (Barberi et al., 1972;Manighetti et al., 1998). At a smaller scale, deformation in Afar seem to have involved the rotation of at least two micro plates (Danakil and Ali Sabieh blocks) sandwiched by the three major plates (Chu and Gordon, 1998). The geologic and tectonic features of Afar have drawn the attention of several researchers, and efforts have been made to give solutions to existing problems applying different geophysical methods. The applications of gravity method in conjunction with other geophysical methods have been effective in mapping crustal thickness variation and in delineating areas of maximum crustal attenuation.

1.3. Objectives

The aim of the thesis is to study crustal thickness variation in the study area. Under this objective, it tries;

-To trace the direction of crustal thinning.

-To estimate the thickness of the crust under selected profiles.

-To infer areas of maximum crustal thinning (attenuation).

-To identify deep seated structures.

CHAPTER TWO

GENERAL GEOLOGY AND VOLCANO TECTONICS

2.1. Geology of the Afar Depression

Afar occupies a triangular shaped topographic basin containing unknown thickness of primarily Cenozoic detrital sedimentary units, evaporites, and volcanics (Barberi et al., 1972; CNR-CNRS, 1975; Christiansen et al., 1975; Varet and Gasse, 1978) (Figure 2.1). In the plateaus adjoining the Afar Depression, Mesozoic and Precambrian rocks out crop, covered on the Ethiopian plateau by extensive Tertiary volcanic flows. The floor of the Depression is covered by several series of Quaternary volcanic with some Pleistocene lacustrine deposits. The Afar Depression is divided into north, central, and south sectors on the basis of its geology and geography (Figure 2.1). ***The northern part of the depression***, with a mean elevation of $\sim$70 m, is dominated by axial volcanic ranges. The $<$1-m.y.-old shield volcanoes of the axial range are typically produced by basaltic fissure eruptions aligned in northwest southeast belts, parallel to the regional tectonic trend of the Red Sea (Barberi and Varet, 1977; Varet and Gasse, 1978). Thick evaporitic deposits are exposed covering several thousand square kilometers. A series of active volcanoes exist in the Depression, providing spectacular outbursts from time to time. The Northern Afar Depression also hosts Miocene to Holocene evaporites and fluvial sedimentary rocks (CNR-CNRS). **The *central sector*** (Figure 2.1) is dominated by graben and horst structures and bounded to the west and east by axial volcanic ranges is occupied by Pliocene flood basalts and Quaternary sedimentary rocks. The flood basalts, which are inter bedded with less common and more silicic layers and volcanic centers, are collectively termed the ‘‘Afar stratoid series’’ (CNR-CNRS [Afar team], 1973; Varet and Gasse, 1978; Barberi and Santacroce, 1980). Available age data indicate that the stratoid series was emplaced between 4.0 and 1.0 Ma (Barberi et al., 1975; Barberi and Santacroce, 1980). Parallel sets of grabens that strike northwest are typical of the region; the mean elevation of Central Afar is 450 m (Figure2.1). The Tendaho graben is one of the largest in the central sector of the Afar Depression.

Southern Afar Rift (Northern Extension of Main Ethiopian Rift)

Southern Afar (Figures1.1 and 2.1), like Central Afar, is dominated by horst and graben structures. Unlike Central Afar, however, the grabens in Southern Afar strike north-northeast, and the topography has a mean elevation of ~700 m. The Tendaho-Goba'ad Discontinuity, a narrow northwest- to west-northwest– trending fault zone, separates Central Afar from Southern Afar (Harding et al., 1990; Ebinger and Hayward, 1996; Hayward and Ebinger, 1996) (Figure1.1). This structure accommodates the change in extension direction between the two sectors and represents the transition from Central Afar to Southern Afar, which is the northern extension of the Main Ethiopian Rift. The prominent north-northeast– trending grabens in the center of Southern Afar are the continuation of the Wonji fault belt, the axial rift zone of the Main Ethiopian Rift (Figure 1.1). The kinematically distinct Gulf of Aden normal faulting pattern (trending due east to east-southeast) is also present in Southern Afar (Figure1.1). It is confined to areas east of the Wonji fault belt in the Gegaas plain and forms major graben bounding faults such as Goba'ad and Dulul (Varet and Gasse, 1978; Abbate et al., 1995). The width and length of grabens in Southern Afar average ~15 km and ~50 km, respectively. These values are typical of the graben systems in Central Afar (Hayward and Ebinger, 1996; Tesfaye, 1999). The parallel development of grabens observed in Southern Afar is also characteristic of Central Afar. The 55 km spacing between volcanic centers in Southern Afar is also within the range of 43 _ 13 km obtained by Mohr and Woods (1976) for the volcanic centers along the Main Ethiopian Rift. These characteristics i.e., width and length of grabens, parallel development of major grabens, and spacing of volcanic centers indicate that Southern Afar shares certain tectonic and/or mechanical or rheological traits with Central Afar to the north and the Main Ethiopian Rift to the south. Pliocene–Holocene lacustrine and fluviatile sedimentary rocks interabedded with basaltic and felsic flows fill extensional basins in Southern Afar (e.g., Renne et al., 1999). Volcanic rocks exposed here include late Miocene (8–6 Ma) Dalha basalts, Afar stratoid series rocks, and Pleistocene volcanic centers (Figure2.1) of the Wonji fault belt (Varet and Gasse, 1978)

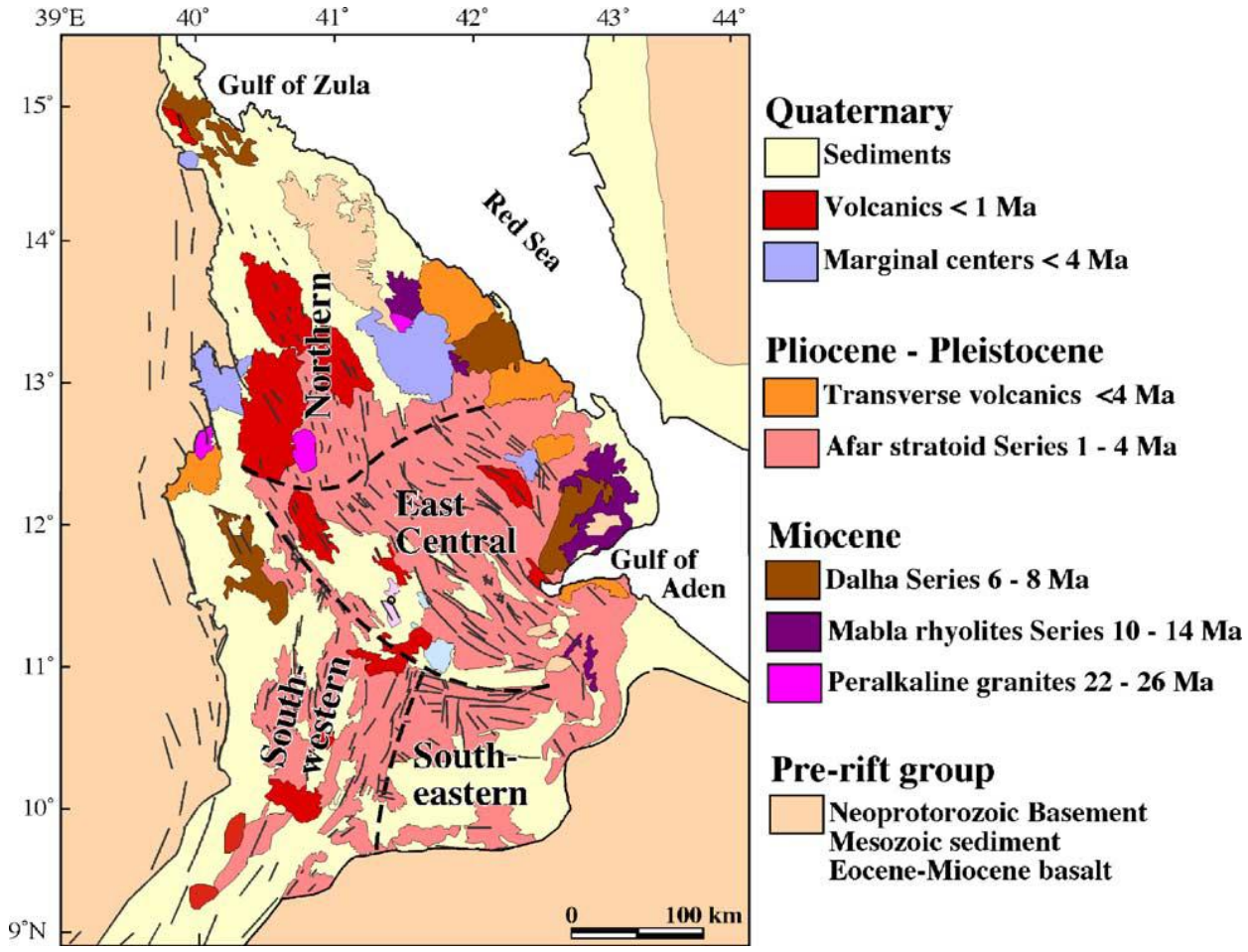

Figure 2.1Geological map of the Afar Depression (after Varet, 1978; Acton et al., 1991). Note the division of the Afar Depression into Northern, East Central, Southwestern, and south eastern – regions.

2.2 Volcano Tectonics of Afar

The southern Red Sea and north-central Afar Depression form two parallel north northwest–trending rift basins, separated by the Danakil horst and related to the separation of Arabia from Africa (Figure1.1). The Afar Depression is exposed at the surface, whereas the Red Sea rift floor is submerged below the sea. The Afar Depression merges southward with the northeast-striking Main Ethiopian Rift and eastward with the east-northeast–striking Gulf of Aden (Figure1.1). The Ethiopian Plateau bounds it on the west. The Main Ethiopian and Afar Rifts are part of the continental East African Rift System (Figure 1.1). These two kinematically distinct rift systems, typical of intra continental rifting, are at different stages of evolution (e.g., Hayward and Ebinger, 1996; Bilham et al., 1999). In the north and east, the continental rifts meet the oceanic rifts of the

Red Sea and Gulf of Aden, respectively, both of which have propagated into the continent (e.g., Manighetti et al., 1998) (Figure1.1). Seismic refraction and gravity studies indicate that the thickness of the crust beneath the Main Ethiopian Rift is ≤30 km (Berckhemer et al., 1975). In Afar the thickness varies from 23–26 km in the south to 14 km in the north (Berckhemer et al., 1975; Makris et al., 1975; Makris and Ginzburg, 1987; Alemu, 1992). The plateau on both sides of the rift has a crustal thickness of 35– 44 km (Searle and Gouin, 1972; Hebert and Langston, 1985). Rates of separation obtained from geologic, geodetic, and plate-kinematic studies indicate 3–6 mm/yr across the northern sector of the Main Ethiopian Rift between the African and Somali plates (Mohr, 1972, 1973; Mohr et al., 1978a, Jestin et al., 1994; Bilham et al., 1999; Chu and Gordon, 1999). The rate of spreading between Africa and Arabia across the Afar Depression is relatively faster, ~16 mm/yr (Chu and Gordon, 1999). The initiation of extension on both sides of the southernmost Red Sea Rift, Ethiopia, and Yemen appears coeval. However, workers have assigned slightly different ages for this event. Dixon et al. (1989) reported an age of 29–23 Ma for the initiation of extension, whereas Menzies et al. (1992) assigned an age of 25–22 Ma for the earliest phase of extension. Ukstins et al. (2002) correlated volcanic and tectonic activities in Ethiopia and Yemen and put the initiation of tectonism at ca. 26– 25 Ma. Ghebreab et al. (2002) reported late Oligocene–early Miocene extension and uplift in Eritrea, with reactivation evident at 10 Ma coincident with rotation of the Danakil horst. The western margins of the Afar Depression are bounded by a seismically active, right-stepping, en echelon system of discontinuous grabens that extend for ~500 km (Figure1.1). The major marginal grabens from north to south are Maglala–Renda Coma, Dergaha- Sheket, Guf-Guf, Menebay-Hayk, and Borkena (Mohr and Rogers, 1966; Mohr, 1967a, 1974a, 1974b). The marginal grabens are interpreted to have been initiated during the early phase of Afar Rift tectonism (Chorowicz et al., 1999; Tesfaye, 1999). The southern termination of the southernmost graben near Kara Kore (latN) is abrupt (Figure1.1).

CHAPTER THREE

PREVIOUS GEOPHYSICAL STUDIES AND RESULTS

Geophysical investigations in and around the Afar Depression have been conducted since the 1960`s. They employed a variety of techniques, but mainly gravity (Makris et al., 1975), magnetic (Girdler, 1970) and Seismic refraction (Berckhemer et al., 1975: Ruegg, 1975). Recently published detailed magnetic data (Courtillot and Le Mouel, 1978) shed light on the structure of the Tajura Bay and its relation to the rest of the depression. This is augmented by new seismicity data (Abdallah et al., 1979; Gouin, 1979) and Mooney et al. (1985) determined the thickness of the oceanic crust in the southern Red Sea (Farasan Island) and on the Arabian Shield from refraction measurements. The results of these investigations were published (Berckhemer et al., 1975, Makris et al., 1975, Behle et al., 1975). (Makris, J. and Ginzburg, A., 1987) reevaluated the available seismic refraction and gravity data using modern interpretation techniques, and new information derived from Magnetic, Gravity, Seismicity and Seismic refraction data.

3.1. Previous Gravity Survey Results

The reevaluation of Bouguer gravity map of Ethiopia (Makris, J. and Ginzburg, A., 1987), produced by Makris (1975), to which were added oil exploration data in southeastern Ethiopia and new data from the Red Sea (Puchelt, 1984) within the frame work of Geodynamics, indicate that the Afar Depression is a transition zone between the continental Rift of Kenya and the present ongoing Sea floor spreading of the Red Sea and the Gulf of Aden. In the Depression itself the crust is greatly attenuated and is underlain by a low velocity (7.4_7.5 km/s) and hence low density, high temperature upper mantle material. However, it is still a continental crust which thins to the northeast and east towards the Red Sea and Gulf of Aden. It is not a newly formed oceanic crust as has been suggested in the past. The trends of the areas of crustal thinning are indicated by the gravity anomalies. The trend of the Ethiopian Rift reaches south Afar where the trend of crustal thinning changes and becomes parallel to the Red sea trend. It is offset en echelon from the spreading area of the Red Sea, which is marked by an alignment of gravity maxima. The Gulf of Aden trend continues west towards the Ethiopian Rift. The gravity trends coincide with

areas of maximum crustal thinning and may thus suggest a possible Triple Junction in development.

Extensive gravity- survey work indicates that mean free air and residual Bouguer anomalies are close to zero over Afar (Gouin,197Oa), which contrasts strongly with the Red Sea and Gulf of Aden (Girdler,1958) .

The fact that similar patterns and contour values exist in both isostatic correction and Bouguer gravity anomaly maps indicate that the Afar Depression is more or less isostatically compensated and the admittance technique can be applied (T. Mammo, 2004) except in areas where admittance technique fails to give satisfactory results. One such case is seen along the Afrera-Dallol traverse where high positive anomalies observed near Afrera (undercompensated). Applying the admittance technique the Moho depth map showed that the crustal thickness of Afar is thin and that it is intermediate between the continental crust and oceanic crust and that there is a further thinning of the crust towards the north and towards the east. The maximum attenuation occurs in the east along the Red Sea coast (43^0E and 11.8^0N) and far north at Dallol.

These are zones where upper mantle materials intrude into the crust. In the southern tip of Afar where the Depression joins the Main Ethiopian Rift there is observed marked crustal attenuation.

3.2 Seismicity of Afar

Epicenteral plots from tele_seismic data show that the greater proportion of strain release in Afar is occurring along the western margin with the Ethiopian plateau (Gouin, 197Oa). No epicenteral concentrations occur along the two volcano tectonic lines mapped by Tazieff and his coworkers in northern Afar. A rather sparse number of epicenters in central Afar may be related to the northward extension of the Wonji fault belt from the main Ethiopian rift (Gouin, 1970a), though Fairhead and Girdler (1970) consider that recent epicenters (1965-1968) are aligned on a WSW projection of the Gulf of Tajura axis across Afar and intercept the Ethiopian plateau in the strongly seismic region of the Borkenna graben. However, the seismicity of Afar marginal graben (Rogers, 1966; Mohr, 1967) is related to the meridional graben faulting subsequent to an initial alignment on WNW-ESE cross-rift faults (Gouin, 1970b). By far the largest of recent Afar earthquakes occurred in the Sedro region of central Afar during spring 1969. This seismicity was centered on N, E and the highest magnitude was 6.2 for the April 5 shock. Gouin and Dakin (1970) observed the effects of oblique- slip movements along N W faults, the sense of shear being sinistral. Fracture lines running approximately E-W were also observed, a direction

coinciding with an alignment of the major epicenters that released strain progressively eastward with time (Fairhead and Girdler, 1970). Sinistral shear along NW-SE faults has occurred during the Quaternary in eastern Afar and the Danakil horst. Such shearing is not immediately reconcilable with the dilation of Afar as part of the Red Sea, though it does offer the possibility of an alternative cause for the formation of the en-echelon structures of northern Afar (Lensen, 1958).

3.3 Seismic Refraction Results

Refraction profiles (Figure.3.1) were measured (Berckhemer et al., 1975) along the main trend of crustal thinning and one west of Addis Ababa in order to compare results within the Depression to a normal continental crust. The crustal structure of the Afar Depression as obtained from the refraction profiles selected by the author departs from the normal continental crustal in both thickness and velocity distribution in the crust and upper mantle. The results show an upper crust with a velocity of 6.1 to 6.2 km/s being observed on all profiles. It is however thinner than normal compared with the thickness of the upper crust on the plateau (18 to 20 km). The total crustal thickness is less than that of a continental crust, being over 20 km over most of the area.

However, one should note that even in the north near Dallol where the thickness of the crust is reduced to 14 km, a 6.1 km/s upper crust is still present. The crustal thickness under the southern extension of the Danakil horst is somewhat greater but not significantly so. The crust throughout the Depression is underlain by an upper mantle with an abnormally low velocity of 7.4 km/s. The unusual structure of the crust as observed on nearly all profiles can be readily explained if one considers the tremendous amount of intrusions which form dikes, sills and extrusives in the Afar Depression thereby modifying the velocity structure. There trends are seen on the structural maps and on the magnetic anomaly maps. Obviously these intrusions follow fault lines and must have reached the surface during the breakup of the crust due to extension (Morton and Black, 1975).

If we consider the lower part of the crust as being made up of granitic blocks invaded by higher velocity upper mantle material, the net effect would be a higher average velocity than that measured over a normal continental crust. The crustal structure of the Djibouti area (Ruegg, 1975) is similar to the rest of the Afar area, having a granitic layer overlying a 6.8 km/s lower crust (referred to as an upper mantle by Ruegg).

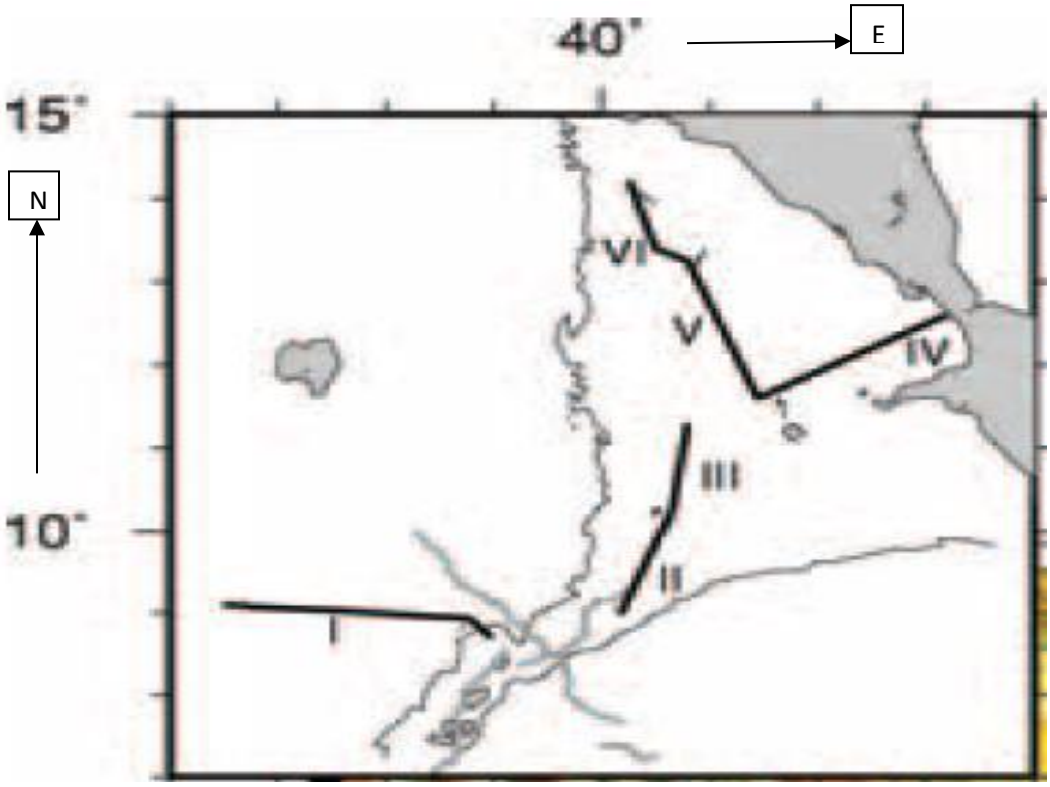

Figure.3.1.Location of the seismic refraction profiles on the western Ethiopian plateau, the northern part of the Main Ethiopian Rift and the Afar depression (from Berckhemer, et al., 1975)

This layer overlies a low velocity (7.1 to 7.4 km/s) upper mantle. Ruegg (1975) has noted a higher than usual Poisson`s ratio of 0.28 to 0.33 compared with 0.25-0.26 for old oceanic and continental crusts. Searle (1975) has found a high ratio across the Afar Depression. These results indicated partially melted upper mantle material. The temperature of the upper mantle material under the Afar is higher than usual, also indicated by the results of the Magneto telluric soundings carried out in the Afar and Djibouti areas (Berktold et al., 1975; Pham Van Ngoc et al., 1981). Berktold et al. (1975) deduced from their observations that the temperatures at the base of the crust in the Afar are of the order of 800^0c to 1000^0c which is twice the normal temperature at a depth of 15 km.

.

CHAPTER FOUR

GRAVITY METHOD

Unlike the active geophysical method of surveying which require transmitting a signal in to the subsurface and record what comes back, the gravity method involves measuring the gravitational field in the earth that is neither generated by the observer nor influenced by anything he does. Like other passive geophysical method gravity survey method make use of natural potential field. The type of information obtainable from gravity or magnetic is quite different from that which seismic prospecting, especially the seismic reflection method can yield. Whereas seismic reflection records give a picture of the sub surface that shows detailed structure of many levels at once. The field observed in gravitational or magnetic prospecting is a composite of contributions from all depths within the usual range of exploration interest, and such contributions can be individually resolved only in special cases. Hence, we can`t expect to obtain the detailed and relatively precise structural picture from gravity or other potential field data that is generally obtainable by seismic methods.

In gravity measurements, the quantity actually observed is not the earth`s true (absolute) gravitational attraction but its variation from one point to another, usually at positions along the earth`s surface which are close together. Such lateral differences can be measured with a much greater degree of precision than the total gravitational field, and field instruments are designed to measure differences in gravity rather than its actual magnitude. The variations in gravity observed through measurements depend only up on lateral changes in the density of earth materials in the vicinity of the measuring point. Thus measurement of the variation, with location, of the gravitational attraction of the earth can provide valuable information about its subsurface geology. This is the basis for the science and practice of gravimetric measurements. Hence gravity surveys look for lateral variations in density to characterize lithology. Many types of rocks have characteristic ranges of density which may differ from those of other types that are laterally adjacent. Density of typical near surface sedimentary rocks is 1.6g/cm^3(from soil to dolomite 1.2-2.9); near surface igneous rocks is 2.9g/cm^3(from rhyolite glass to peridotite 2.2 - 3.5g/cm^3).

This enables as to relate an anomaly in the earth`s gravitational attraction to a buried geological feature; such as a salt dome or other diaper, which has limited horizontal extent.

4.1. Fundamentals of Gravity Method

The gravity survey method is based on the following two Newton`s laws;

1) Universal law of gravitation, which states that the attraction force between two point masses M and m is inversely proportional to the square of the separation distance r and directly proportional to the product of the two masses.
   Mathematically:

   (4.1)

   where r is the distance between the two masses, G is the universal gravitational constant, which from experiment has a value $G=6.67\times10^{-8}$ dyne.cm^2/gm^2=6.67×10^{-11}Nm^2/kg^2 and F is the force on m due to M or vice versa.

   Note: A point mass specifies a body that has very small dimensions (i.e. the mass can be considered to be concentrated at the center of mass.)

2) Second law of motion, which states that the acceleration, **a** on an inertial mass, m produced by a net external force, F is directly proportional to the net external force that produce it.
   Mathematically:

   (4.2)

4.2. Gravitational Acceleration

Combining Newton`s second law of motion (Equation.4.2) and the law of universal gravitation (Equation.4.1), the gravitation acceleration of a mass, m due to the attraction of mass M, a distance r away can be given by:

(4.3)

The acceleration being the force acting on a unit mass is a conventional quantity used to measure the gravitational field acting at any point. All masses located at the same position in the field are subject to the same gravitational acceleration.

4.3. Units for

In the SI unit system, the dimension of acceleration is meter per Second Square (m/sec.^{2}). In the cgs system of units, the dimension of acceleration is centimeter per Second Square (cm/sec.^{2}). Geophysicists refer to this unit as the gal (in honor of Galileo, who conducted pioneering research on the earth`s gravity.). Sub units used in gravity measurements include: MilliGal (mGal), micro Gal (μGal), micro meter per Second Square (μm/sec^2), which is referred to as the gravity unit (g.u.)

(1g.u=0.1mGal).

4.4. Gravitational Potential

As the intensity of gravity, magnetic, or electric fields depends only on position, the analysis of such fields can often be simplified by using the concept of potential.

The potential at any point in a gravitational field is defined as the work done by the gravitational force to move a unit mass from an arbitrary reference point (usually at an infinite distance) to a point in question. Let's consider the figure below. A unit mass, m is brought to a point, a distance, r from M by the gravitational force: .

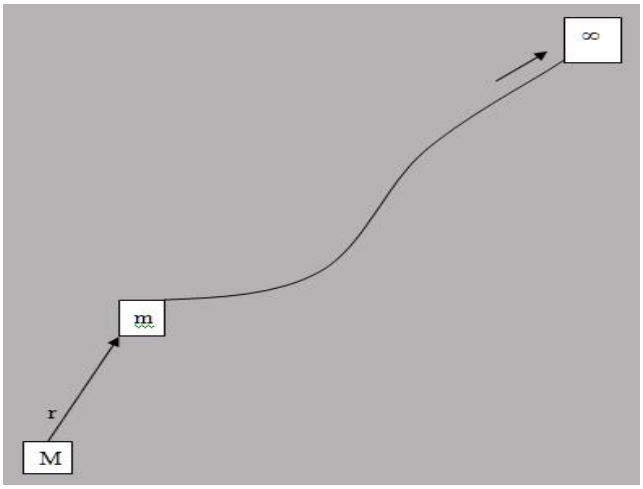

Figure.4.1 Dependence of gravity field with distance from the center of the earth

, where

=) = (4.4)

The work done per unit mass, = (potential). (4.5) or

The potential can be given by: .

This implies (4.6)

For a multidimensional potential, (gradient of the potential) (4.7)

4.5. Potential Field Equations

The divergence theorem (gauss` theorem) states that the integral of the divergence of a vector field over a region of space is equivalent to the integral of the outward normal component of the field over the surface enclosing the region.

Mathematically, we have (4.8)

Where is normal to the surface.

If there is no attracting matter contained within this volume, the integrals are zero and

(4.9)

But from equation (4.7), the gravitational field is the gradient of a scalar potential, so that

(4.10)

This shows that the gravitational potential satisfies Laplace`s equation in free space. If on the other hand, there is a particle of mass, m within the volume, and in particular if we consider it to be at the center of a spherical surface of radius r, then the integral

=) = (4.11) this result holds regardless of the shape of the surface and the position of the particle within the surface. If the surface encloses several particles of total mass, m, we can write;

,where V is the volume. If this volume is made very small, enclosing a point in the region, we may remove the integral sign to give; where is the density at the point. Then using equation (4.7)

(4.12)

which is Poison`s equation. From equations (4.10) and (4.12) we see that the gravitational potential satisfies Laplace`s equation in free space and Poison`s equation in a region containing attracting material.

4.6. Gravity Field of the Earth

Consider a small mass, m moving with a velocity, V on the surface of the earth rotating with angular velocity, as shown below.

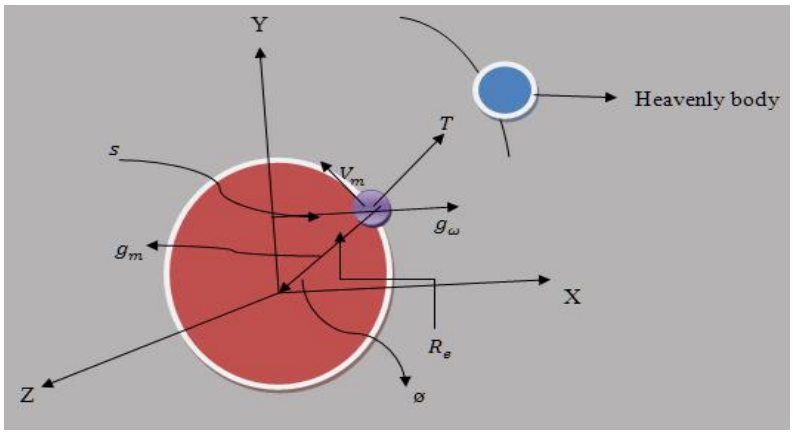

Figure 4.2.Forces per unit mass acting on a mass, m located on the surface of the rotating spherical earth.

From figure (4.2), the resultant force per unit mass (acceleration) acting on the mass, m is

given by: T, where is the attraction force per unit mass acting on m due earth`s mass,  is the centrifugal force per unit mass acting on m due to earth`s rotation with angular speed, is the Coriolis force acting on due to its linear velocity, on the earth`s surface and is the tidal force per unit mass acting on due to mass attraction of other heavenly bodies.

- If we assume the earth to be spherical in shape with radius and mass , then from equation (4.3) we have the mass gravitational acceleration :

$=$ (4.13)

-The centrifugal acceleration is given:

(4.14) .

This can also be written as:

(4.15)

The centrifugal acceleration has two components:

The radial component or the component along of is

= and

The component of tangent to the earth`s surface is (4.16)

= =

The Coriolis acceleration (**C**) resulting from the Coriolis force is given by:

2() (4.17)

If the mass is at rest (V= 0) on the surface of the earth, then **C=0.**

Note: the Coriolis force should be considered in air born and marine measurements. But, we can ignore the Coriolis force when we make gravity measurements standing on the solid earth.

It is not easy to express T with a simple formula due to the variation in position and a number of heavenly bodies causing it.

Hence, in actual gravity survey on land, the effect of C and T on is usually considered negligible. Therefore, refers to the combined effect of both earth`s mass gravitational acceleration and rotational (centrifugal) acceleration i.e.

. (4.18)

The tangential component of the doesn`t have a contribution to the measured gravity. Therefore, the acceleration due to gravity is the sum of the mass gravitational acceleration, and the radial component of the centrifugal acceleration,

If the radial inward direction is positive, then the centrifugal acceleration (radial component) will be negative.

Mathematically;

- (4.19)

This equation shows that reduces the acceleration of gravity by an amount

. It also indicates that the variation of on the earth`s surface depends on.

Equation (4.19) gives at the poles where and

(4.20)

- at the equator where

Equation (4.20) implies that polar gravity is greater than equatorial gravity.

The difference between polar gravity, and equatorial gravity, is given by:

(4.21)

For a spherically symmetric earth of radius cm, the calculated amount of, where, rad /sec, which is known to a high degree of accuracy from astronomy. By using gravity observing apparatus (pendulum, gravimeter etc.) on the real earth, the observed value of polar gravity and equatorial gravity are:

and .

The above results show that the difference in the observed values i.e. for the real earth is different from the theoretically computed values for a spherically symmetric earth. This disagreement between the difference in the observed and theoretically computed values of at polar and equatorial regions of the earth indicates the shape of the earth is distorted from a spherical shape because of rotation. The rotational distorted earth is:

- Flattened at the poles because of maximum resulting in short polar radius **c.**
- Bulged at the equator because of minimum resulting in long equatorial radius **a**

4.7. The Earth`s Figure and Gravity

The earth`s shape and gravity are intimately associated. The spherical earth model is confirmed to be an excellent first approximation to earth`s shape that is adequate for solving many problems. But Newton, who used a hydrostatic argument to account for the polar flattening suggested a spherical model of the earth flattened at the poles. The figure of the earth is the shapes of an equipotential surface of gravity in particular the one that coincides with mean sea level. The best mathematical approximation to the figure of the earth is an oblate ellipsoid, or spheroid (Figure.4.3).

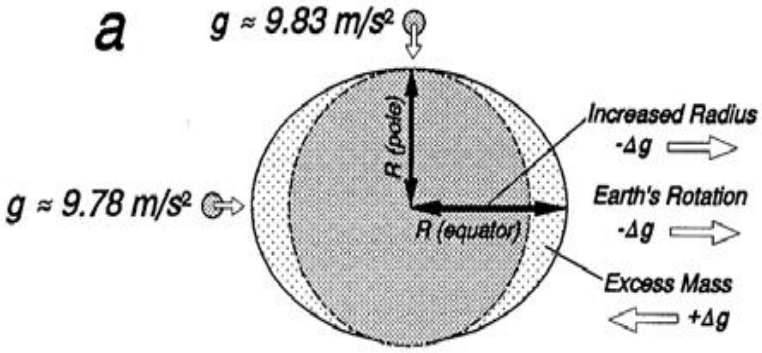

Figure.4.3. An oblate spheroid flattened at the poles and bulged at the equator.

The precise determination of the dimensions of the earth (i.e. its polar radius (**c**) and equatorial radius (**a**)) is the main objective of the science of geodesy. It requires an exact knowledge of the earth`s gravity field, the description of which is the goal of Gravimetry.

Modern analysis of the earth`s shape are based on precise observations of the orbits of artificial earth satellites. These data are use to define a best fitting oblate ellipsoid, called the international reference ellipsoid. In 1930, Geodesists and Geophysicists at the international union of Geodesy and Geophysics (IUGG) meeting defined an optimum reference ellipsoid based on the best available data at the time. The dimensions of this figure have been subsequently refined, as more exact data have been available. In 1980, Geodesists and Geophysicists at the IUGG meeting agreed on a reference ellipsoid whose equatorial radius **'a'** is 6378.136km and polar radius **'c'** is 6356.751km. The radius of the equivalent sphere is found from to be 6371.000km. Compared to the best fitting sphere, the ellipsoid is flattened by about 14.2 km at each pole and at the equator;

it bulges by about 7.1km. The polar flattening is defined as the ratio: . The flattening of the optimum reference ellipsoid, defined in 1930, was exactly. This ellipsoid and the variation of gravity on its surface served as the basis of gravimetric surveying for many years, until the era of satellite Geodesy and highly sensitive gravimeters showed it to be too in exact. In 1980, the value of the flattening was revised to .

4.8. Gravitational Potential of the Ellipsoidal Earth Model

On a stationary spherical earth model, the gravity and gravitational potential is given by

, and

(4.22)

, respectively where on the surface

But on a rotating globe, these constant values must be modified to account for flattening and centrifugal effects both of which change with latitude.

For the derivation of the gravitational potential of the ellipsoidal earth, the earth`s gravitational potential or the Geo potential W at the earth`s surface consists of the mass gravitational potential generated by all masses of the earth (disregarding the effect of the atmosphere) and the rotational (centrifugal) potential **Φ** resulting from the radial component of the centrifugal acceleration acting on these masses because the masses are rotating:

(4.23) where , the mass gravitational potential, and

Φ =

= where (4.24)

Hence, the explicit form of the earth`s gravitational potential or the Geo potential W on the earth`s is: (4.25)

The change in the earth`s potential, when the test mass, is displaced by an amount along is equal to the work done by the earth`s gravitational field given by:

$= -$ (4.26)

If the test mass is moved in a direction perpendicular to (i.e.), then

(4.27)

This result defines a family of equipotential surface, each of which can be determined by assigning a definite (particular) value to the constant. Of these family of equipotential surfaces, the ellipsoid and the geoid are two of such equipotential surface of the earth that are constructed to coincide with a theoretical earth model (ellipsoid) and physical earth model (geoid). Geophysicists and geodesists consider these two surfaces to represent the average shape of the rotationally distorted real earth.

4.9. Level surfaces, Plumbs Lines, Geoid and Ellipsoid

The level surfaces, where W (x, y, z) = = constant, are called equipotential surfaces. Corresponding to each equipotential surface, there is a constant and a perpendicular force to the surface.

The total differential of the potential is given by:

$= ($

$=$ but

$=$, along the equipotential surface S,

$0 =$, as both and

$\Longrightarrow$ is Perpendicular to.

This results means that the earth`s gravitational field (plumb lines) are perpendicular to the equipotential surfaces.

An ellipsoid (theoretical earth model) is an equipotential surface corresponding to mean sea level (constant). It is described by its equatorial radius (**a**), polar radius (**c**) and the flattening ().

The Geoid (physical or natural earth model) is also an equipotential surface corresponding to mean sea level. It is defined under land areas as the surface that would be assumed by the top of the water in a narrow sea level canal if it were extended in land across a continent to connect one ocean to another. The Geoid is by definition everywhere perpendicular to the direction of the plumb lines.

4.10. Reference Ellipsoid and Theoretical Gravity on the Reference Ellipsoid

To determine the gravity field of the earth at a point we must know its shape and density distribution. For describing the earth`s shape, one usually uses a reference ellipsoid of revolution with z axis coinciding with the axis of rotation and the plane coinciding with the equatorial plane. We assume that the ideal reference ellipsoid which is related to the mean sea level surface with excess land masses removed and ocean deeps filled, is an equipotential surface of a normal gravity field (theoretical gravity field). The direction of gravity at a point is defined as perpendicular to the equipotential surface through the point. This defines the vertical at the point, while the plane tangential to the equipotential surface defines the horizontal. A consequence of the ellipsoidal shape is that the vertical direction is generally not radial, except on the equator and at the poles.

On a spherical earth model, there is no ambiguity in how we define latitude. It is the angle at the center of the earth between the radius and the equator or it is the complement to the polar angle (ϴ). This defines the geocentric latitude, ϕ`. However the geographic latitude, ϕ in common use is not defined in this way. It is found by geodetic measurement of the angle of elevation of a fixed star above the horizon. But the horizontal plane is tangential to the ellipsoid, not to a sphere.

The vertical direction (i.e. the local direction of gravity) intersects the equator at an angle ϕ, that is slightly larger than the geocentric latitude ϕ`. The difference (ϕ`- ϕ) is zero at the equator and poles and reaches a maximum at a latitude of , where it amounts to only.

The international reference ellipsoid is the standardized reference figure of the earth. The theoretical value of gravity, on this rotating ellipsoid can be computed by differentiating the gravity potential, (equation. 4.25), that is, =. This yields the radial and the transverse components of gravity, which are then combined by performing the required mathematics to determine the variation of the theoretical gravity value, that is normal to the ellipsoid surface and given by

(4.28)

Where is the value of gravity at the equator: , are constants determined by adjustment. Equation (4.28) is known as the normal gravity formula. The normal gravity formula also known as theoretical gravity formula is very important in the analysis of gravity measurements on the earth, because it gives the theoretical variation of normal gravity, with latitude on the surface of the reference ellipsoid.

Recent studies on the orbit of satellite have provided precise value for the determination of the constants based on precise determination of ***a*** and ***b*** has resulted in an explicit gravity formula revised several times.

In 1930, the international association of geodesy (IAG), a sub unit of the international union of Geophysics and Geodesy (IUGG) held in Stockholm, Sweden adopted the formula known as the 1930 international gravity formula given by:

MGal (4.29)

.

In 1967, the IUGG adopted a revised theoretical gravity formula given by:

= 978031.85(1+0.0053024) MGal (4.30) with .

For practical work measurements of gravity is carried on the physical equipotential surface (i.e. Geoid). The gravity potential on the reference geoid is given by:

(4.31)

For theoretical work gravity is calculated on the theoretical equipotential surface; i.e. ellipsoid.

The gravity potential on the reference ellipsoid is given by:

(4.32)

Letting that the ellipsoid and geoid coincide at mean sea level, we have

(4.33)

The value of gravity observed, on the geoid surface is determined by: and the value of gravity calculated on the ellipsoid surface is theoretically determined by:

The gravity anomaly is defined as the difference between and as given by:

(4.34)

Gravity anomalies are developed as a consequence of the differences in density distribution of the earth, particularly in the upper layer known as the crust. Therefore they reflect the internal constitution of the crust and indicate the presence of various geological structures connected with the dislocation of rocks of different densities. This enables us to study the internal structure of the earth and for gravity prospecting.

CHAPTER FIVE

GRAVITY DATA AND REDUCTION

5.1. Gravity Data

Gravity data is collected through gravity surveying, conducted by making gravimeter readings at many locations in an area of interest. Other measurements and observations, other than gravity, must also be made to describe the position of each observation site. Especially important are latitude and elevation, because these values enter directly in to the computation of gravity anomalies. Furthermore we must note the time when each reading is made so that corrections for gravimeter drift can be determined.

The choice of gravimeter observation sites depends on the geologic features that are of particular interest and on the accessibility of the area. The separations between these sites depend on the size of the geologic features that are of particular interest: ranging from intervals closer than one or two kilometers to several kilometers apart.

The object of a survey is to measure the values of gravity, at the observation sites where changes in gravity, between these places and a conveniently located reference site, called a base station, where gravity has already been determined. The base station should be one of the sites in the **1971 International Gravity Standardization Net (IGSN71).** If none of these sites are close to the survey area, it may be necessary to determine the reference value of gravity, at a more conveniently located base station using gravimeter measurements adjusted to the IGSN71.

5.2. Factors that Affect the Gravitational Acceleration

The spatial variations in gravitational acceleration expected from geologic structures can be quite small. Because these variations are so small, we must now consider other factors that can give rise to variations in gravitational acceleration that are as large, if not larger, than the expected geologic signal. These complicating factors can be subdivided into two categories: those that give rise to temporal variations and those that give rise to spatial variations in the gravitational acceleration.

- **Temporal Based Variations** - These are changes in the observed acceleration that are time dependent. In other words, these factors cause variations in acceleration that would be observed even if we didn't move our gravimeter.
- Instrument Drift - Changes in the observed acceleration caused by changes in the response of the gravimeter over time.
- Tidal Affects - Changes in the observed acceleration caused by the gravitational attraction of the sun and moon.
- **Spatial Based Variations** - These are changes in the observed acceleration that are space dependent. That is, these change the gravitational acceleration from place to place, just like the geologic affects, but they are not related to geology.
- Latitude Variations - Changes in the observed acceleration caused by the ellipsoidal shape and the rotation of the earth.

- Elevation Variations - Changes in the observed acceleration caused by differences in the elevations of the observation points.
- Slab Effects - Changes in the observed acceleration caused by the extra mass underlying observation points at higher elevations.
- Topographic Effects - Changes in the observed acceleration related to topography near the observation point.

5.3. Tide and Drift Correction

In order to determine the drift correction gravity observations are made around loop (Figure Below).That is, before starting to make gravity observations at the gravity stations; the survey is initiated by recording the relative gravity at the base station and the time at which the gravity is measured. Proceeding to move the gravimeter to the survey stations (1- 16), where relative gravity and the time at which the reading is taken, is measured (Figure below). After some time period, usually on the order of an hour, we return to the base station and re measure the relative gravity at this location. Again, the time at which the observation is made is noted. If necessary, we then go back to the survey stations and continue making measurements, returning to the base station every hour. After recording the gravity at the last survey station, or at the end of the day, we return to the base station and make one final reading of the gravity.

To determine the drift correction for each observation site, we need to make a plot of readings observed at the base station as a function of time, then linearly interpolate between the points so that the drift curve can be prepared from this plot and the drift correction for each observation site can be read from the drift curve at the respective observation time.

In addition to the instrumental drift (internal cause), there is a time variation of gravity resulting from the variation in the gravitational attraction of the sun and the moon as their positions change with respect to the earth. The corrections can be calculated from knowledge of the relative positions of the sun and the moon with respect to the earth. However, because the variation is smooth and relatively too slow, usually it is included in the instrumental drift correction.

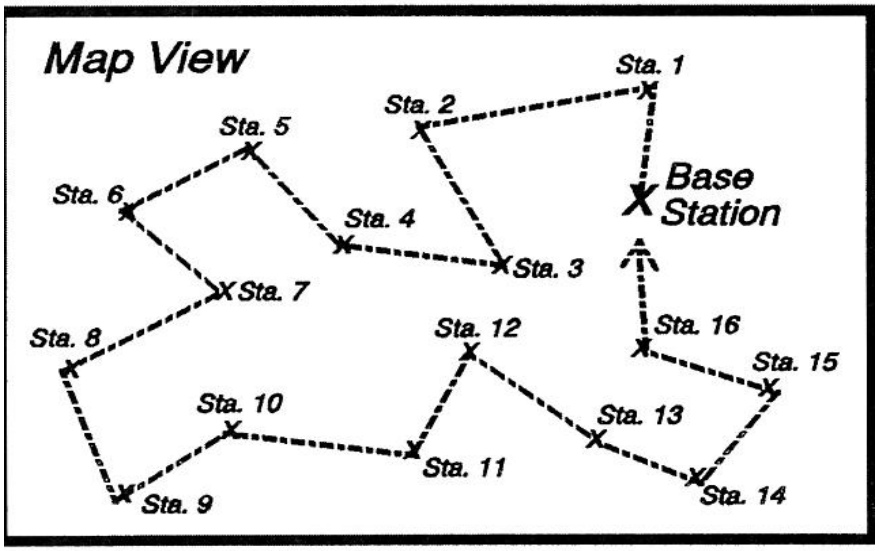

Figure 5.1, Map showing the loop method of gravity survey

5.4. Latitude Correction

Due to its spherical shape, the earth is flattened at the poles and bulged at the equator. Because of flattening, polar radius is smaller than equatorial radius and hence a greater polar gravity than equatorial gravity. Generally, gravity increases with latitude. The variation of gravity with latitude over the surface of an ellipsoidal earth can be given in (Equation 4.28).

Partial differentiation of equation (4.28) with respect to gives the latitude correction for small scale studies as;

() = (5.1)

where

Hence, for the mean latitude, of a given survey area the variation in the theoretical gravity for every one meter distance travelled in a N_S direction is the latitude correction given by:

. This correction is added to as we move towards the equator.

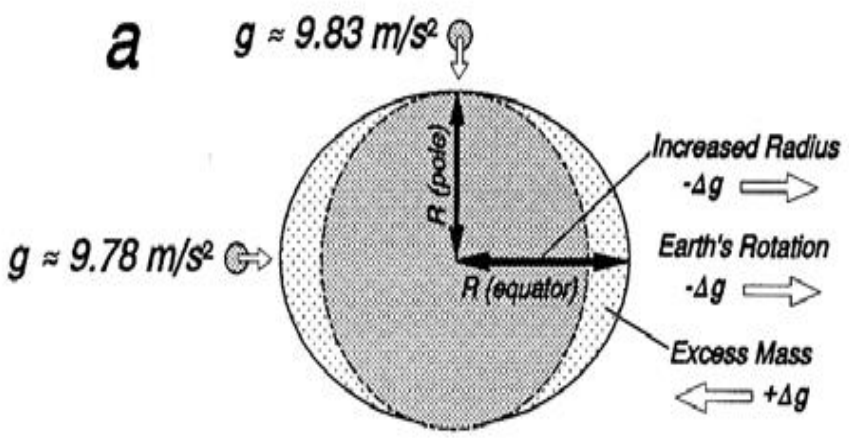

Figure.5.2.Effect of Spheroidal earth on gravity field

How large is this correction to our observed gravitational acceleration? And, because we need to know the latitudes of our observation points to make this correction, how accurately do we need to know locations? At latitude of 45 degrees, the gravitational acceleration varies approximately 0.81 mGals per kilometer. Thus, to achieve an accuracy of 0.01 mGals, we need to know the north-south location of our gravity stations to about 12 meters.

5.5. Free Air Correction

Accounts for the decrease in gravity with distance from the center of the Earth, recall:

. The free air correction accounts for only changes of gravity with height. So it is necessary to correct for changes in elevation between stations to reduce observations to datum surface (Mean sea level Geoid).

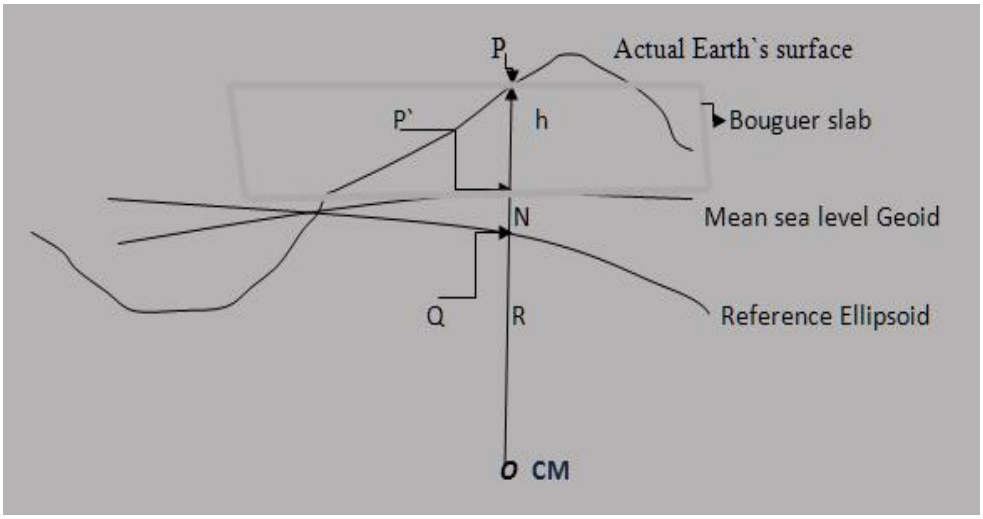

Figure5.3) shows the Reference ellipsoid, Mean sea level geoid and the actual earth`s surface.

Gravity on the actual earth`s surface = on the mean sea level geoid = and on the reference ellipsoid =. The free air correction () is therefore the decrease in gravity due to the height () above the mean sea level geoid (Figure5.3).

This can be given by:

= but by the binomial expansion

= retaining only the first two terms.

,

where,

Inserting = and , the free air correction for measured in meters is:

(5.2)

The free air correction is added to the gravity reading when the station is above the geoid and subtracted when below it. Therefore the free air reduced gravity is given by:

5.6. Bouguer Correction

The Bouguer correction accounts for the attraction of the material between the station and the datum plane (Mean sea level Geoid) that was not considered in free air correction. The rock mass in between the station and the datum plane is treated as an infinite horizontal slab having uniform density. Corrections based on this simple slab approximation are referred to as the Bouguer Slab Correction. It can be shown that the vertical gravitational acceleration associated with an infinite slab can be written simply as:

(5.3)

Where the correction is given in mGals, is the density of the slab in **g/cm^3**, and is the elevation difference in meters between the observation point and elevation datum. The sign of the Bouguer correction is applied in opposite sense to the free air correction i.e. it is subtracted when the station is above the geoid and vice versa. This effect may be difficult to calculate because one does not know the density. Furthermore, if the elevation change is confined to a small region, like going up a hill, then the infinite slab is an inappropriate description of the intervening mass. Under this circumstance the actual topography must be considered and another effect, the terrain effect, is included. Conventional practice is to apply the Bouguer correction first and, the terrain correction. The Bouguer reduced gravity is given by:

5.7. Terrain Corrections

When Bouguer correction is inadequate, also use terrain correction. It allows for surface irregularities in the vicinity of the station (i.e. accounts for variations in the observed gravitational acceleration caused by variations in topography near each observation point). With considerable topographic relief the infinite Bouguer slab is not a good model for the intervening mass between the reference elevation and the point of observation. The actual gravitational effects must be calculated numerically for the masses above and below the slab surface.

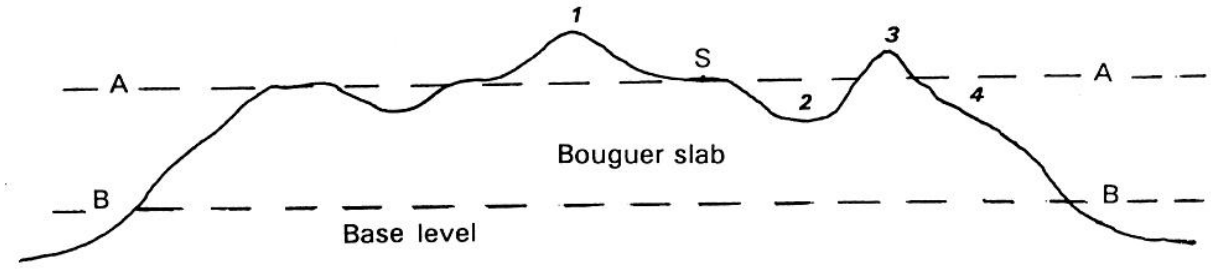

Figure 5.4.Bouguer and terrain corrections. The Bouguer correction refers to the gravity effect of the intervening plate mass between station, **S** and the base level **B**. The terrain correction takes in to account the effect of topographic rises (1, 3) and depressions (2, 4).

In the above figure, mass excess adjacent to the observation point (1, 3) reduce the value of and the mass deficit adjacent to the observation point (2, 4) which also reduces the value of Similar to the Bouguer reduction it is necessary to determine the appropriate density values of the surrounding lithologic units to carry out terrain reduction. The terrain corrections are difficult to do in very rugged terrain because the nearest features have the biggest effect. Choosing the density is also a problem but an iterative process is used until the corrected data shows no correlation with the topography.

.There are several methods for calculating terrain corrections all of which require detailed knowledge of relief near the station and a good topographic map extending considerably beyond the survey area. **Rectangular grid** and **Hammer segments** are approaches to terrain correction. Both use elevation differences between the station and the surround. If we consider the hammer method, the whole area in the vicinity of the observation point is represented by concentric circles and radial lines, making sectors whose areas increase with distance from the centre.

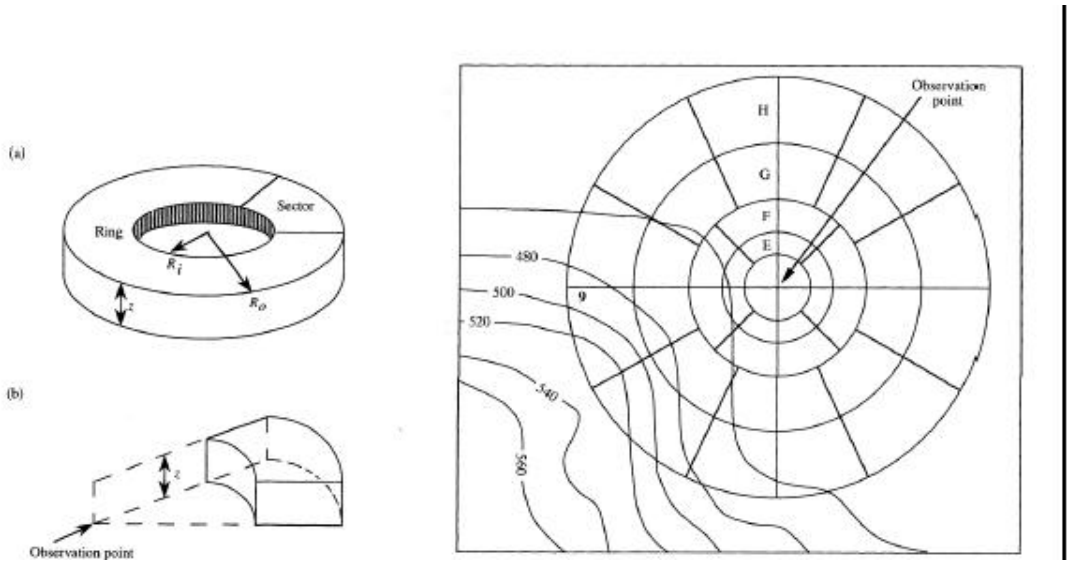

Figgure5.5. shows Hammer sectors and rings to determine terrain correction.

The gravity effect of a single sector () can be calculated from the formula:

where, ,,

and **&** are outer and inner radii respectively.

The terrain correction is the sum of all the sectors. Therefore, if we have number of sectors, the total terrain correction will be:

(,)

The terrain correction is positive regardless of whether the local topography consists of a mountain or a valley region. As a result the terrain correction is always added to the station reading. The terrain reduced gravity is given by:

5.8. Determination of reduction density

Why do we need rock density? As stated in the previous sections, it is necessary to determine the appropriate density, which we call the reduction density, to carry out the Bouguer correction as well as the Terrain correction.

In many areas, near surface densities are sufficiently homogeneous for an average density value to be obtainable from a few well spaced determinations. In others, there are such sharp local variations in lithology, where the use of an average density value can introduce considerable error.

When one wishes to determine density directly, representative samples of rock from surface out crops, mines, or well cores and cuttings may be collected for measurement with a Pyknometer or a Schwarz or jolly balance. Direct sampling of surface rocks over a large survey area is a formidable task and the density estimate so made may not even be representative of the rock material at moderate depths. This fact has necessitated an indirect method (in situ method) to be devised for the determination of density of surface rocks.

Nettleton has proposed an indirect means of density determination (Figure5.6) which may be more satisfactory for gravity reductions than direct measurements on small samples. The Nettleton method of density determination involves running a density profile with a gravimeter over a topographic feature, such as a small hill or a valley, with dimensions measured accurately. The observed gravity values are then reduced and plotted with a series of different density values for the Bouguer and Terrain correction. The appropriate density (reduction density) value is that density value which yields a Bouguer anomaly with a list correlation (positive or negative correlation coefficient, r) with the topography (Elevation).

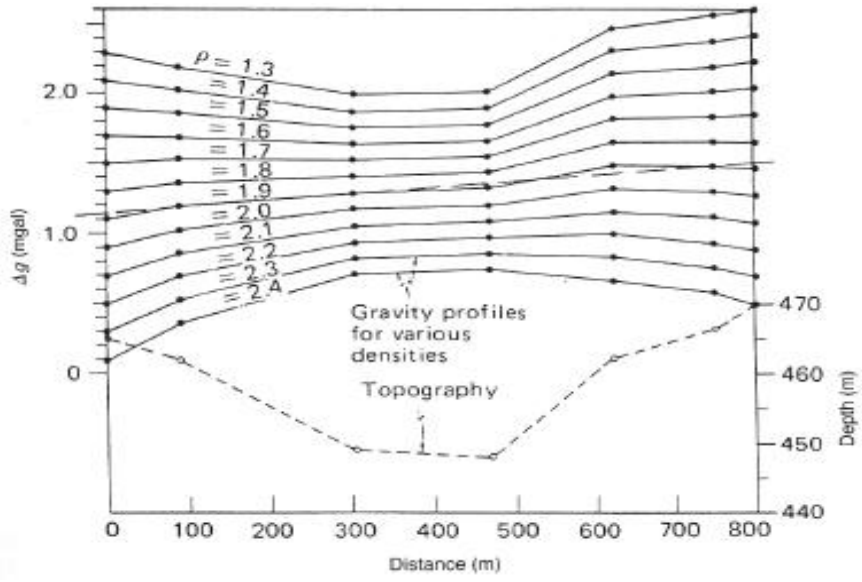

Figure.5.6. shows a gravimetric method for measuring the surface density (Nettleton method). The criterion for the actual density is that which gives a reduced gravity profile with no visible correlation with the topography. The indicated density of 1.9 g/cm^3(1900 kg/m^3) is an average value for the topographic feature sampled. (Modified from Nettleton, 1971)

5.9. Gravity Anomaly

The word anomaly implies deviation from the normal. Gravity anomalies (Free – air and Bouguer) are geophysical tools up on which effects of geology on the earth's gravity field can be detected.

If is the measured gravity value at station elevation above the geoid, it should be reduced to sea level (geoid) to compare it with, the theoretical value on reference ellipsoid of the same latitude . Therefore the gravity anomaly at a station is defined by,

Where; **is** the gravity anomaly; is the measured gravity value of a station reduced to geoid surface, after the temporal and spatial corrections have been applied; **is** the theoretical gravity of the station at latitude .

In order to get the desired anomaly that is caused by geologic structure, we have to reduce the measured gravity value, for the corrections that we have mentioned before.

5.10. The Free Air Anomaly ()

It is the difference between the free air reduced gravity and the theoretical gravity values both at the same latitude. This can be given as:

.

This does not correct for topography. Onshore free air anomaly map is similar to topography. Hence, it is mainly used for offshore.

5.11. The Simple Bouguer Anomaly *()*

It is the difference between the Bouguer reduced (only for the Bouguer slab) gravity and the theoretical gravity at the same latitude. This can be given by:

5.12. The Complete Bouguer Anomaly *()*

This is the difference between the terrain reduced and the theoretical gravity values at the same latitude.

where is the value of the computed Terrain correction.

Assuming these corrections have accurately accounted for the variations in gravitational acceleration they were intended to account for, any remaining variations in the gravitational acceleration associated with the Terrain Corrected Bouguer Gravity, can now be assumed to be caused by geologic structure.

5.13. The Bouguer Anomaly Accuracy

The accuracy of the Bouguer anomaly is determined by the amount of errors which were propagated from the measured value to the Bouguer anomaly. Error on Bouguer anomalies arises

from the precision in determining latitude, elevation, reduction density, the observed gravity and the accuracy of the instrument used in the survey.

Since the Bouguer anomaly is given by: , then the total differential of the Bouguer anomaly gives as the standard error .

Where,, , , are the gravity observation, elevation, density and latitude errors respectively and are called standard errors.

The variance of the standard errors, , can be computed from the law of propagation of errors for uncorrelated observations as:

This being the standard error, the overall mean square error, of the Bouguer anomaly becomes;

where is the systematic or bias error of the gravity anomalies.

CHAPTER SIX

GRAVITY DATA, DATA PROCESSING AND INTERPRETATION

6.1. Acquisition and Distribution of Gravity Data

The gravity data used for this study were obtained from the Ethiopian Institute of Geological surveys (EIGS). The dataset consists of 1237 measurements conducted in Afar, distributed as shown in (Figure6.1). All the gravity stations surveyed by the Ethiopian Institute of Geological survey were tied to the IGSN71 (International Gravity Standardization Net 1971; Morelli et al., 1971), which is located in Addis Ababa.

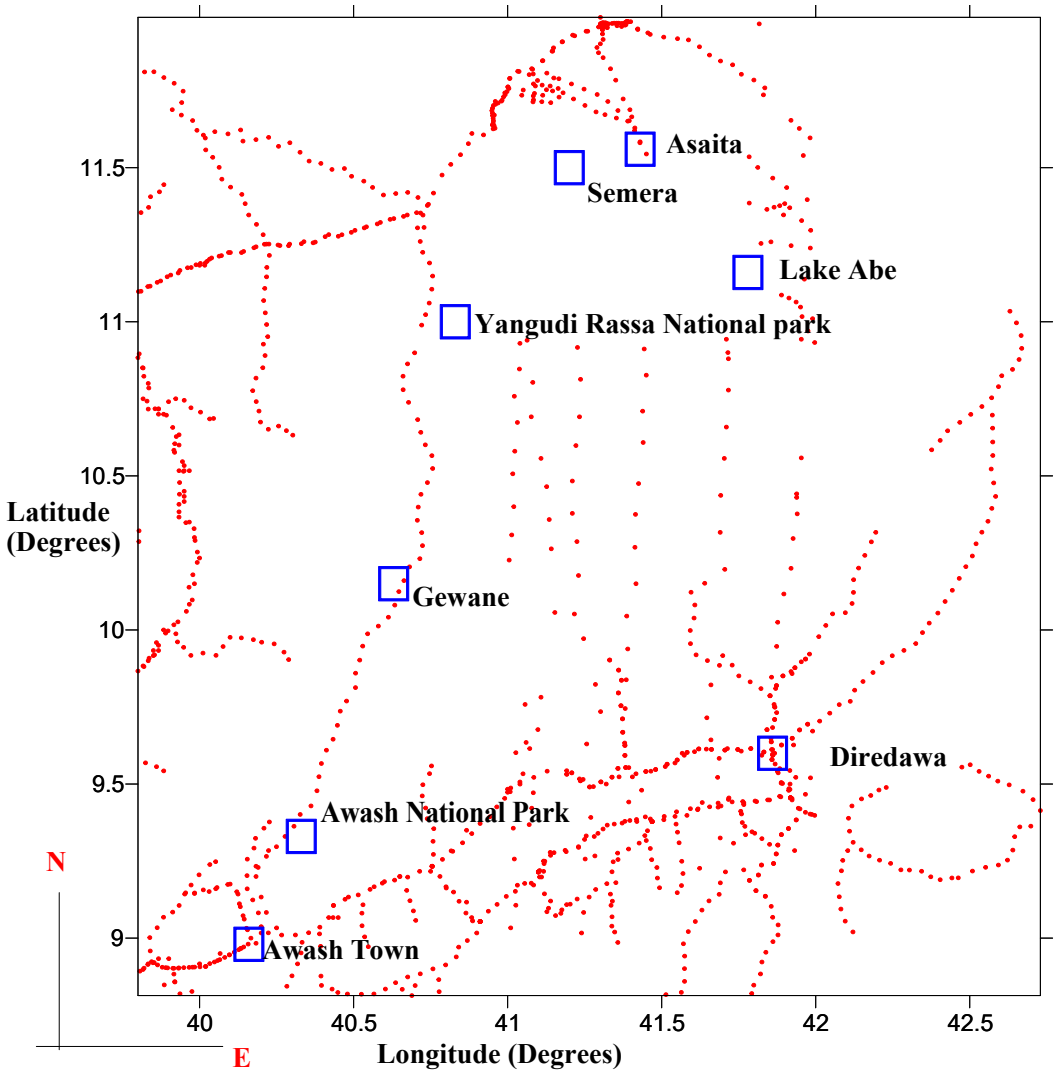

Figure.6.1. Station location where measurements are made

6.2. Gravity Data Analysis and Qualitative Interpretation

The standard corrections (drift, tidal, latitude, free air, Bouguer, and terrain) discussed in chapter five has been made. The data were reduced to mean sea level geoid with a uniform crustal density of 2.67g/cm^3. The Bouguer gravity anomaly was calculated using the Geodetic Reference System of 1967 (GRS67). The gravity data, after all the above correction(drift, tidal, latitude, free air, Bouguer and terrain) has been made, is Gridded using the geostatic Gridding method called kriging (Cressie, 1991; Journel and Huijbregts, 1978), which interpolates the data in a regular grid. The regularly gridded data was mapped in contour maps. The Bouguer gravity map (Figure6.2) is generated using 'surfer 8' software (Golden Software Inc., Colorado, U.S., 2002).

6.2.1. Bouguer Gravity Anomaly Map

The Bouguer anomaly map produced (Figure6.2) has a contour interval of 7mGal. The Bouguer anomaly map varies between – 219.6 to – 4.8mGal. Data points are also plotted for the validity of the plots.

A first glance at the Bouguer anomaly of the study region shows a clear distinction between the Afar depression and the surrounding (the western Ethiopian plateau, the south east plateau and the opening of Afar to the Main Ethiopian Rift (MER) i.e. southwest apex of the triangular depression).

Lower gravity values including the relative minimum gravity anomaly is observed over the western Ethiopian plateau while the other relatively minimum Bouguer gravity occurs over the southeastern plateau. Intermediate Bouguer gravity is observed over the region where the Afar depression opens to the MER, except at a localized region where higher values like that observed in Afar is revealed. This localized higher gravity anomaly has a NE-SW trend, which may be related to crustal thinning (extension) resulting from the separation of the Nubian plate from the Somalian plate. (Mammo, 2004) also found a marked crustal thickness at the southern tip of Afar where the MER joins the depression. Relatively higher values are observed over the depression, where the maximum Bouguer anomaly occurred. This maximum Bouguer anomaly occurs in the form of two separated anomaly patterns trending in NNE-SSW to NE-SW.

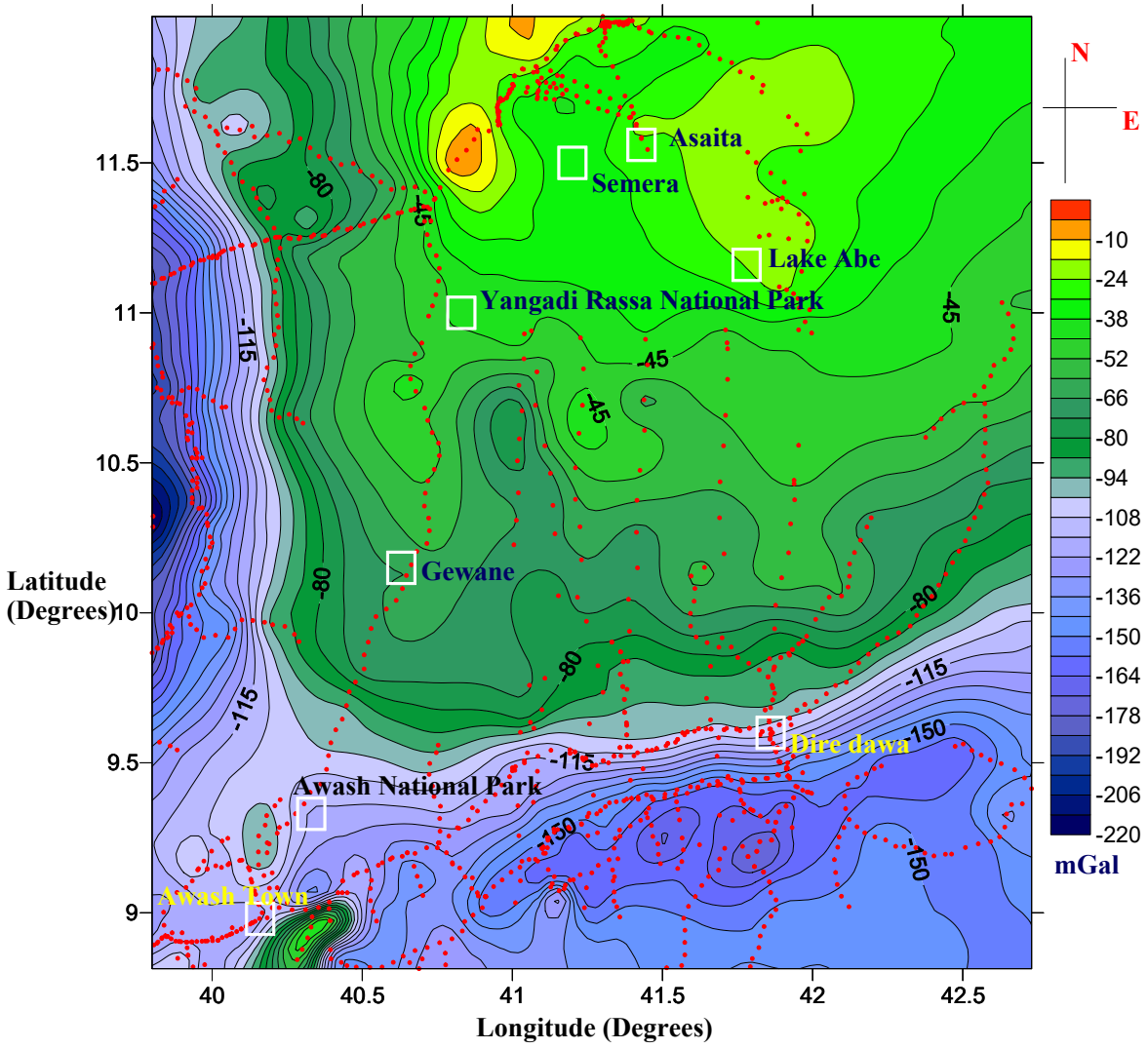

Figure 6.2.Bouguer Anomaly Map

Generally, there seems a negative correlation between the Bouguer anomaly and topography of the study region, where minimum values are located areas of maximum elevation and vice versa. The minimum value occurred over the western plateau while the other lower value is over the southeast plateau (Figure6.3)

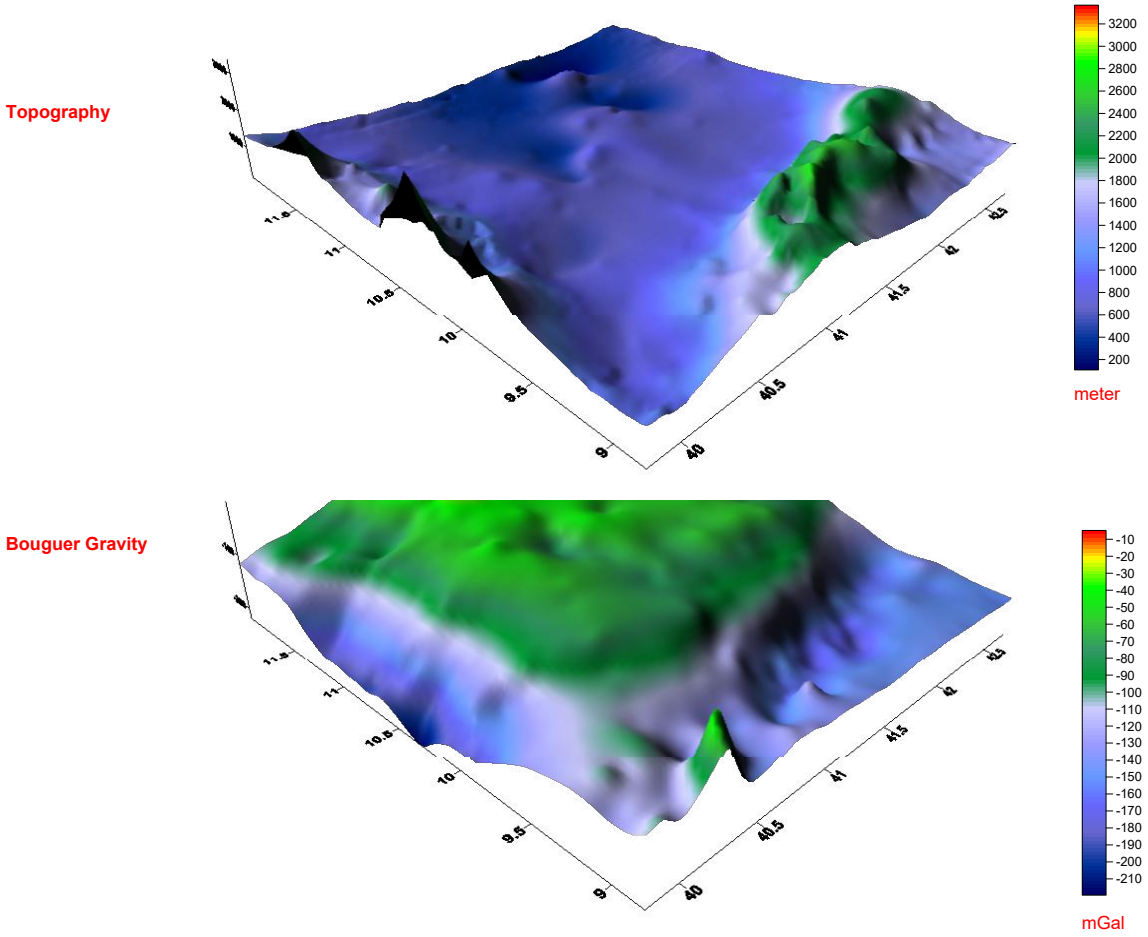

Figure 6.3.Surface map of Topography versus Bouguer Gravity

6.3. Filtering of Gravity Data

Upward continuation and horizontal gradient filters are applied to the Bouguer gravity.

6.3.1 Upward Continuation

This is based on the concept that if gravity values are known anywhere on the Earth`s surface, gravity at any higher elevation can be calculated from these values. This process, which has a similar effect as a low pass filter suppresses short wave lengths and accentuates long wave length anomalies. The gravity field is upward continued to suppress higher wave numbers that are related to near surface bodies. This allows all deep seated structures to become clearer. As the elevation increases more of the shorter wave length anomalies are suppressed.

The Bouguer anomaly map (Figure6.2.) is filtered progressively by higher upward continuation filters (i.e. 10km, 20km and 30km) to give the upward continued residual anomaly maps (Figure6.4). This shows that the highest gravity anomaly observed, followed an ellipsoidal trend with the major axis in the NE to SW, progressively intensified and the contrast between the Afar depression and the plateaus in the west and South East becomes sharp. This may be due to the fact that the causative body for the highest Bouguer gravity observed may be deeper.

3D gravity inversion showed that the higher gravity value in Afar is caused by a thin (23km) and denser crust (Tiberi et al., 2005). The elliptical shape may be related to the accommodation zone for the change in extension direction between the central and the southern Afar.

6.3.2. Total Horizontal Gradient

This operation measures the rate of change of field in the x and y directions and creates a resultant grid. The amplitude of the horizontal gradient (Cordell and Grauch, 1985) is expressed as: (6.1)

Where and are the horizontal derivatives of the gravity field in the x and y directions.

This horizontal gradient method has been used for many years to locate density or susceptibility boundaries from gravity data (Cordell, 1979) or magnetic (as pseudo gravity) data (Cordell and Grauch, 1985). This has the effect of highlighting high gradient areas such as might occur at faulted boundaries. It is also useful for delineating structural trends. The image map of the horizontal gradient is shown in (Figure6.5).

Maximum gravity gradient occurred at the southwest apex and south of the study region, which may be related to faulted structures. N-S trending relatively higher gradient, which coincides with the western boundary of Afar, may be attributed to the bordering escarpments while the other relatively higher gravity gradient (trending in ENE-WSW) coincides with the boundary of Afar and southeastern plateau, which could also be attributed to south eastern escarpment.

High gradients in the central and north western part of the study area may be attributed to localized structures (probably graben structures).

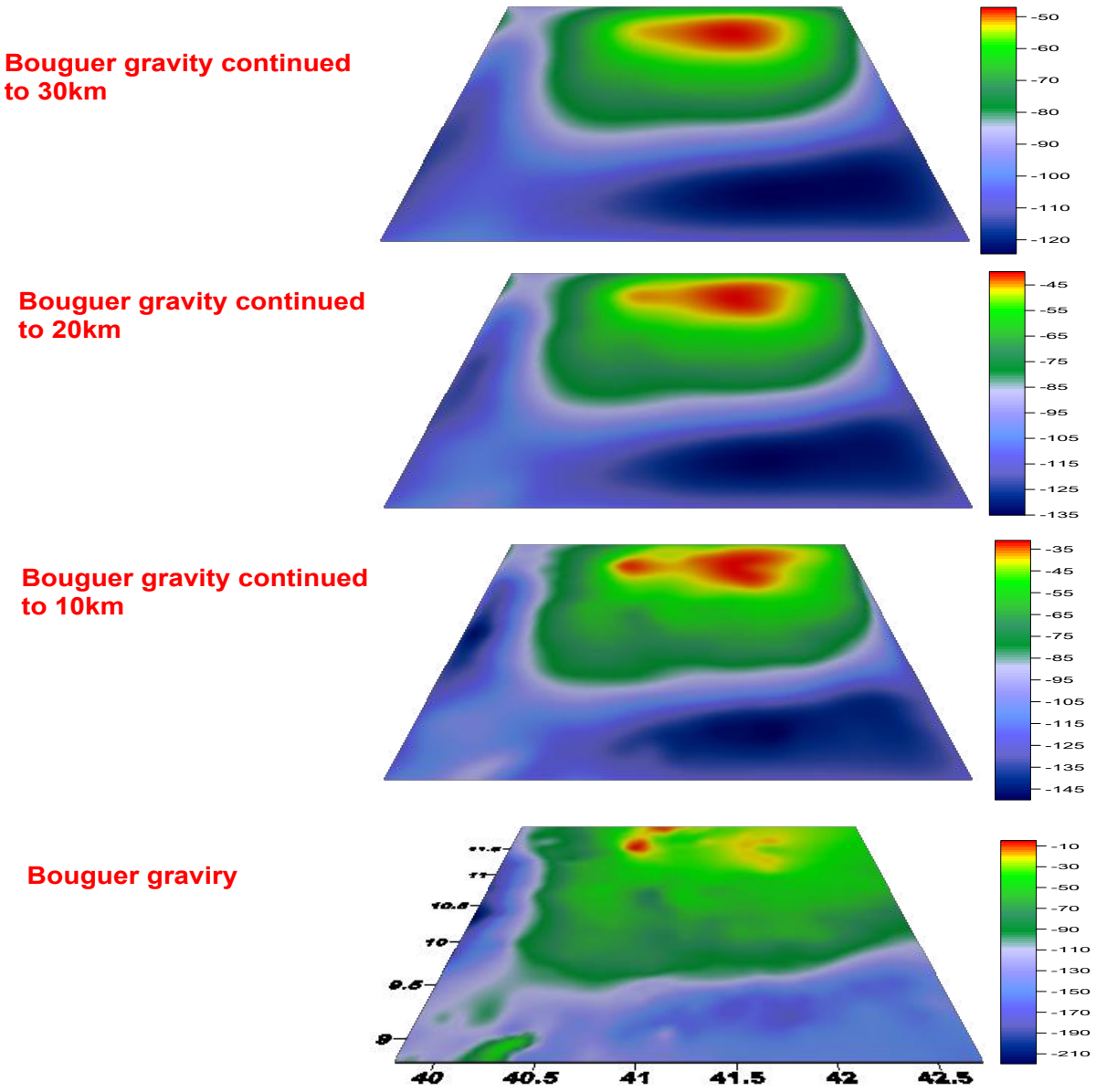

Figure.6.4.Result of upward continuation filter

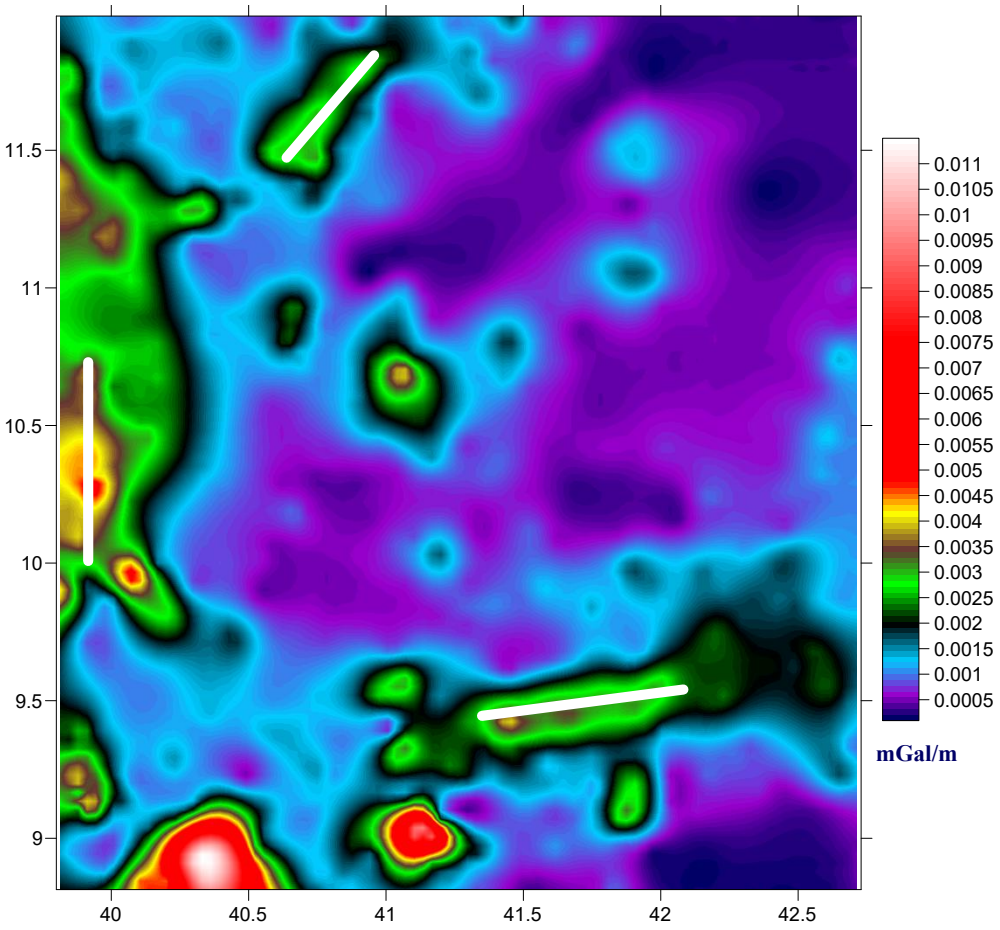

Figure.6.5. Plot of horizontal gradient

6.4. Regional-Residual Anomaly Separation

In order to study the gravity anomaly in Afar in detail, a residual gravity anomaly map was constructed. There are a variety of techniques that can be used to estimate the regional gravity anomaly including polynomial fitting, wave length filtering, etc. Here in this thesis, Second order polynomial fitting is used to approximate the regional field. The residual gravity is obtained by subtracting the regional field from the Bouguer gravity. The separated anomalies (Regional and Residual) created by these mathematical expressions are useful in a qualitative sense to infer the origin of the anomalies.

6.4.1. Residual Gravity Map

The residual anomaly map (Figure6.6) has a contour interval of 5mGal. The residual gravity value varies between -91.8 to 82.1. The residual anomaly map shows negative values over the

western Ethiopian plateau and the southeastern plateau. This may be related to thicker crustal masses (lower density) under the plateaus. The maximum gravity value is observed at the bottom of the southwest apex of the study region, where higher gradient also observed. This may be a site of geologic structure which brings denser material to the surface. Higher gravity values follow a trend of NE-SW up to about 10^0N and N-S trend where it becomes parallel to the main escarpment. This elongated residual gravity maximum follows NNE-SSW trend (centered with higher values) further north of the study region. This elongated higher (positive) residual value coincides with the trend of crustal thinning (Makris and Ginzburg, 1987). Other higher (positive) gravity values are seen at the northwest apex (NNW-SSE trending) and E-W trending higher gravity in the eastern part of the study region. Higher positive anomaly is revealed in the southeast apex and southwest apex, which was masked in the Bouguer anomaly. The central, northwestern and the rest of the study region show residual anomaly values zero and near zero. Extensive gravity survey work also indicate that mean free air and residual Bouguer anomalies are close to zero over Afar (Gouin, 1970a), which contrasts strongly with the Red sea and Gulf of Aden (Girdler, 1958). Smaller localized positive and negative gravity anomalies are observed, which may be attributed to the local geology.

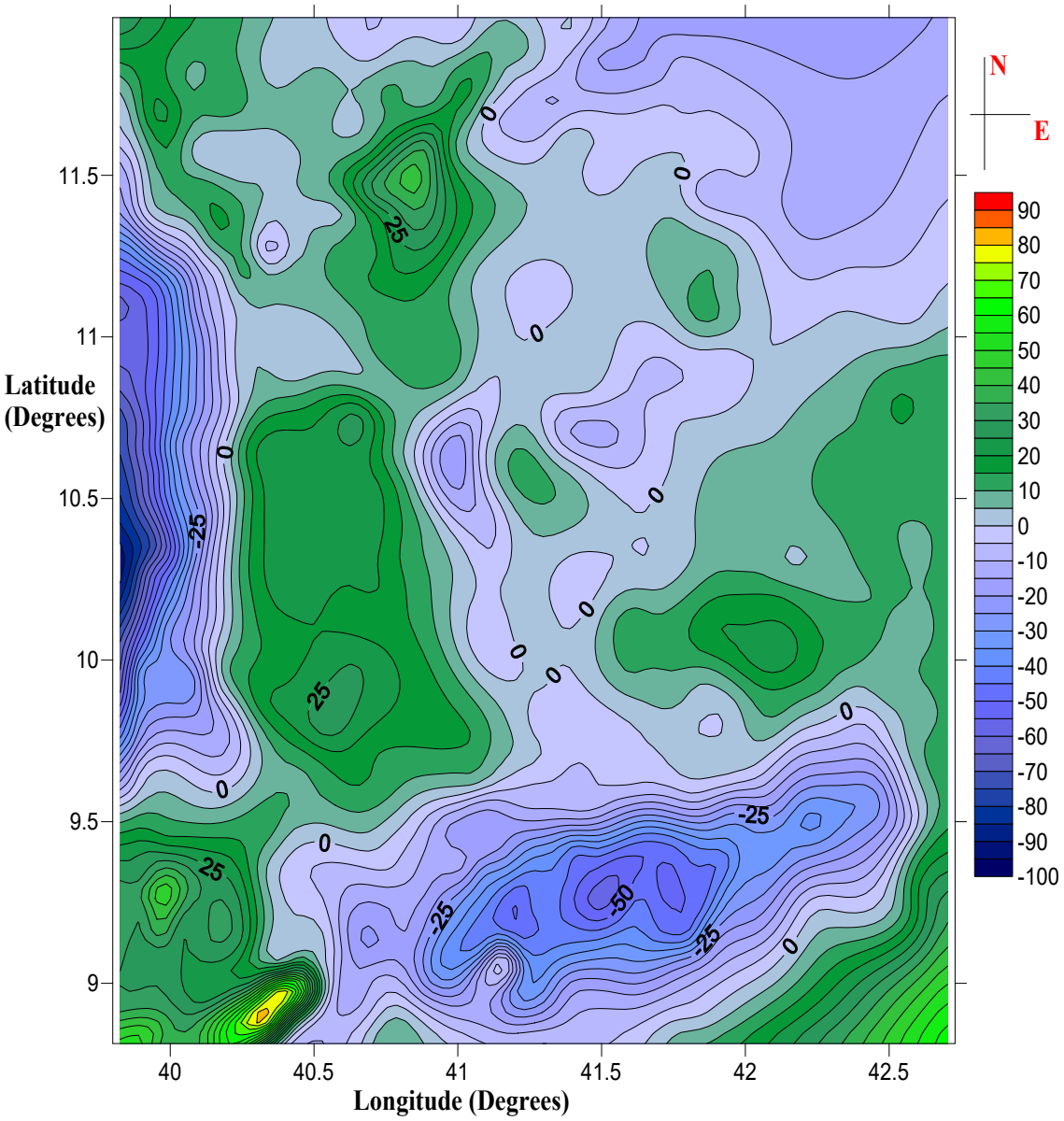

Figure.6.6. Residual Anomaly map

To reveal the details of the anomaly trends and for a better resolution, the Image map of the residual gravity (shown in Figure6.7) is included here.

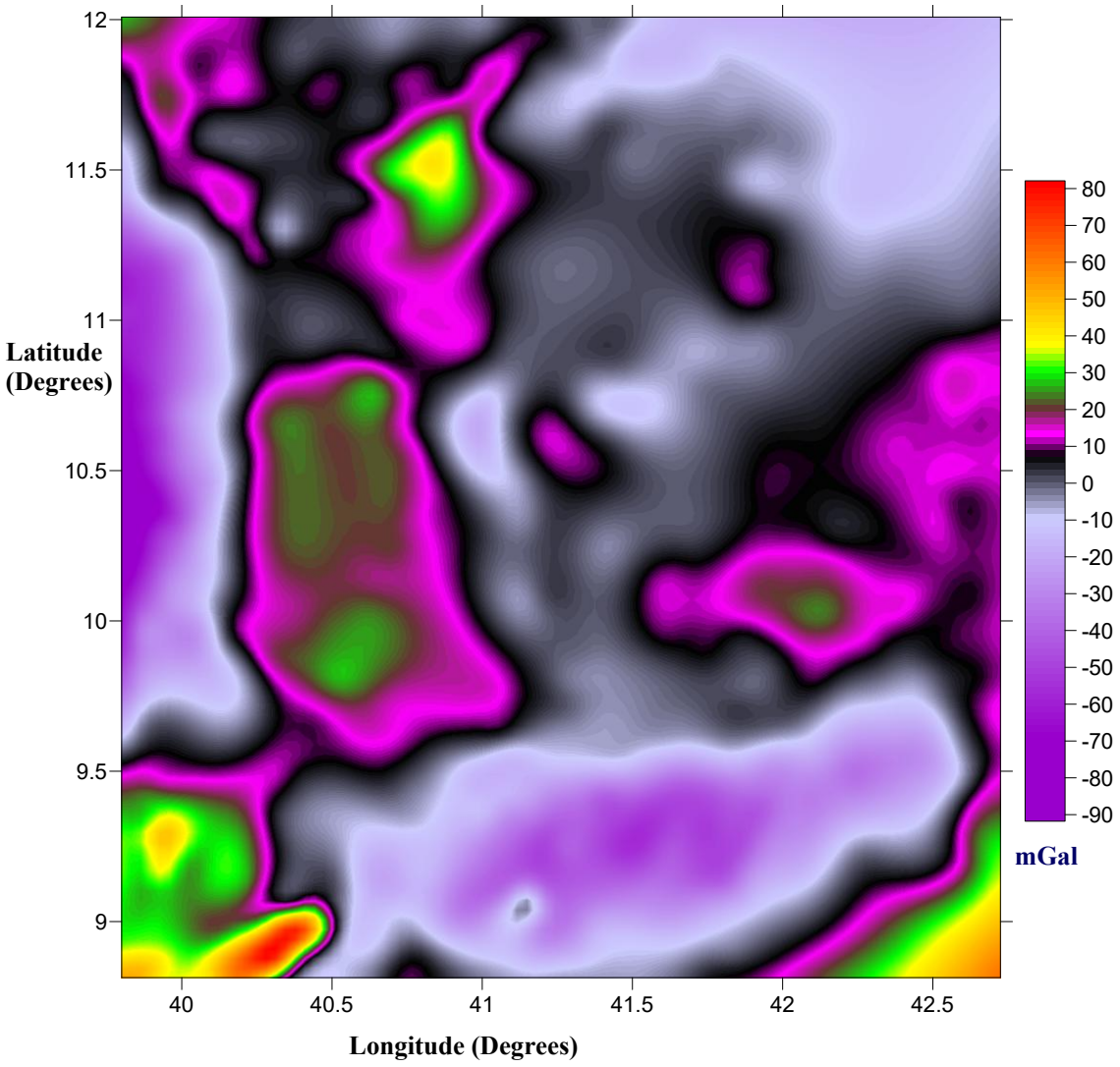

Figure.6.7. Image map of the residual gravity

6.4.2. Regional Anomaly Map

The regional anomalies map (Figure6.8), obtained from second order polynomial fitting, have a contour interval of 10mGal. It varies from -207.9 to -6.8mGal. The regional anomaly is dominated by NE-SW trending contours with increasing value toward NE. relatively higher regional values separate the depression from the rest of the study region, where relatively lower regional values are observed. The maximum and minimum regional values are observed at the northeast End and southeast End of the study region. Even though, relatively higher regional values are observed in the Afar depression, still the values are negative. The regional absence of a strong positive regional values agrees with the Wegner`s (1929) observation that the elevation of

most of Afar above sea level points to the presence of sialic masses beneath the lava cover. There is an inverse relation between the topographic relief and regional gravity field in the study region. This is associated with isostatic compensation of the topographic relief by low density material at depth (Makris et al., 1975).

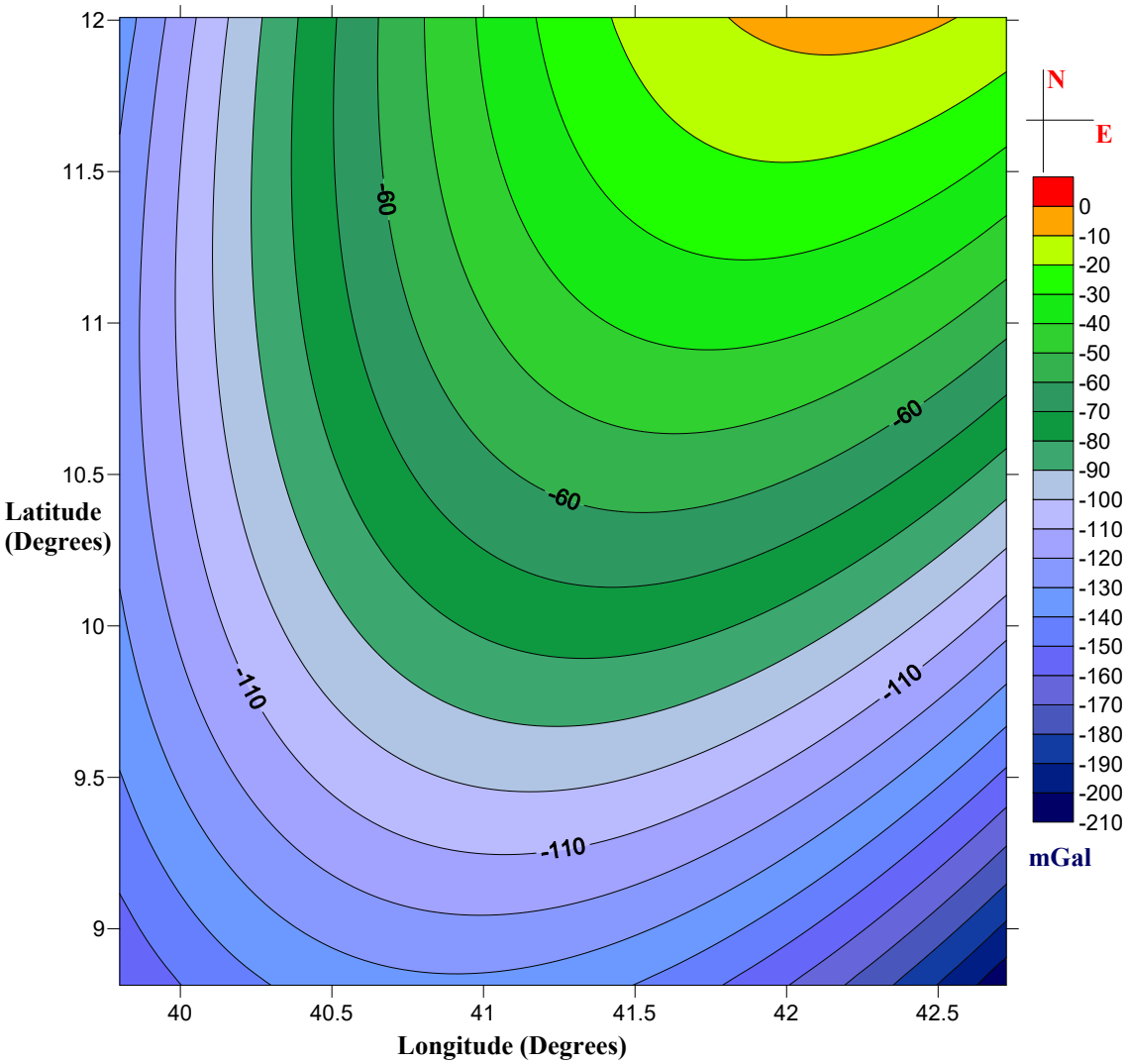

Figure.6.8. Regional Bouguer gravity of the study area

6.5. Euler Deconvolution

Euler deconvolution assists the interpreter by indicating portions of the data of interest, which can then be modeled in detail. No particular geological model is assumed; a range of elementary gravity distributions are used as the source of the anomalies. The input is a gravity signal profile, and the output is a plot of the location of the different types of sources present. Sources are

characterized by their structural indices,, which correspond to the rate of decay of the field strength with distance from the source. Some examples are given below;

Structure	Structural index ()
Sphere	2
Horizontal cylinder	1
Fault(small step)	0

(Table.6.1)Some examples of structure and structural index

2D form of Euler`s equation can be defined (Reid, 1990) as;

Where, and are the derivatives of the field in the *x* and *y* directions, is the structural index value that needs to be chosen according to a prior knowledge of the source geometry. By considering three or more neighboring observations () at a time (an operated window), source location () and can be computed by solving a linear system of equations generated from equation (6.2). Then by moving the operated window from one location to the next over the anomaly, multiple solutions for the same source are obtained. We have assigned several structural index values and found that structural index of (1.0) gives good clustering solutions. Figures6.10 (a) and (b) shows the results of the Euler method from the residual data taken along the profiles BB` and CC` (Figure6.9)

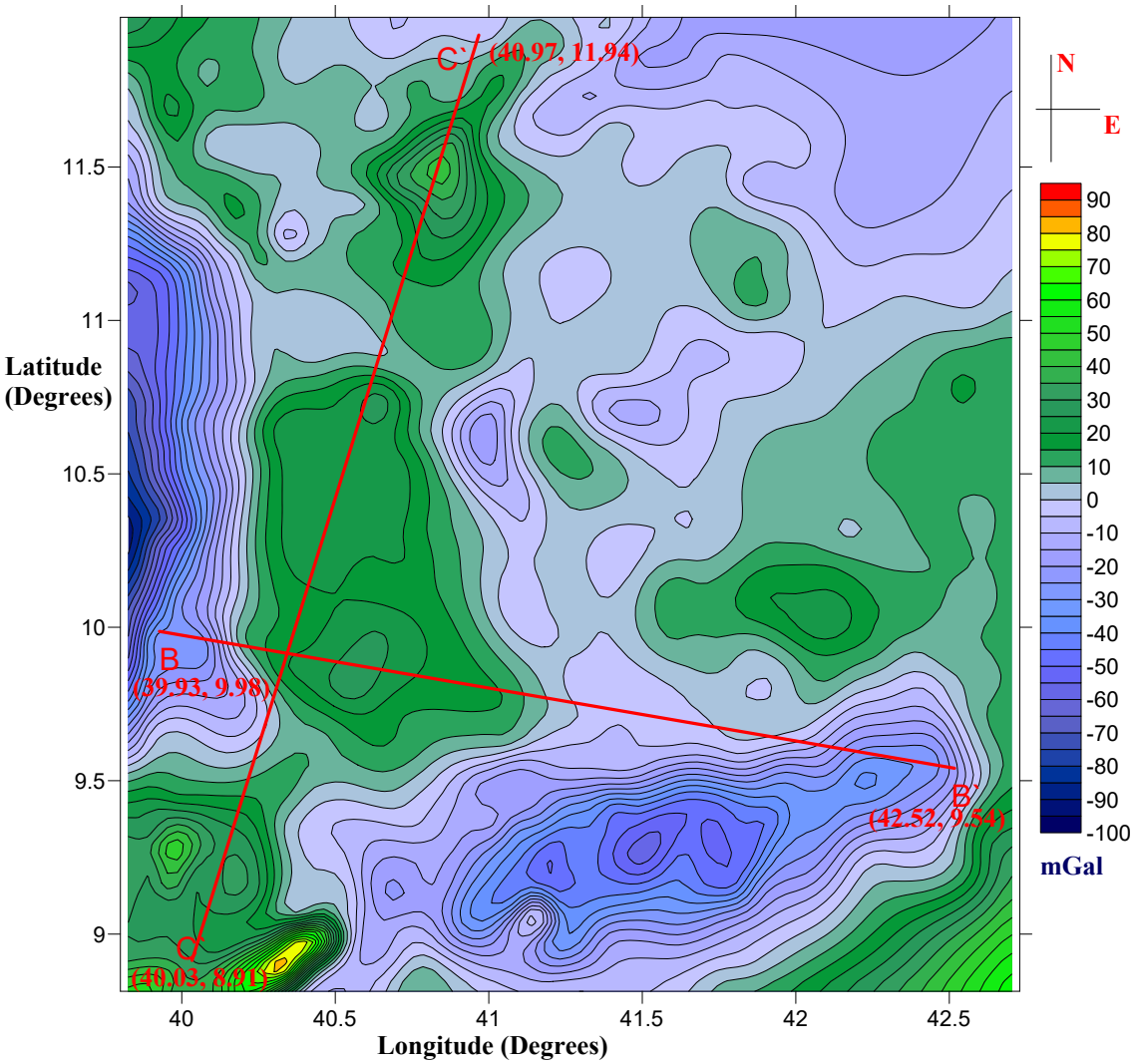

Figure.6.9 Profiles taken on the residual gravity

The Euler solutions Figures10 (a) and (b) indicate that the depth of source distribution is not more than 30km for both profiles, CC` and BB`.

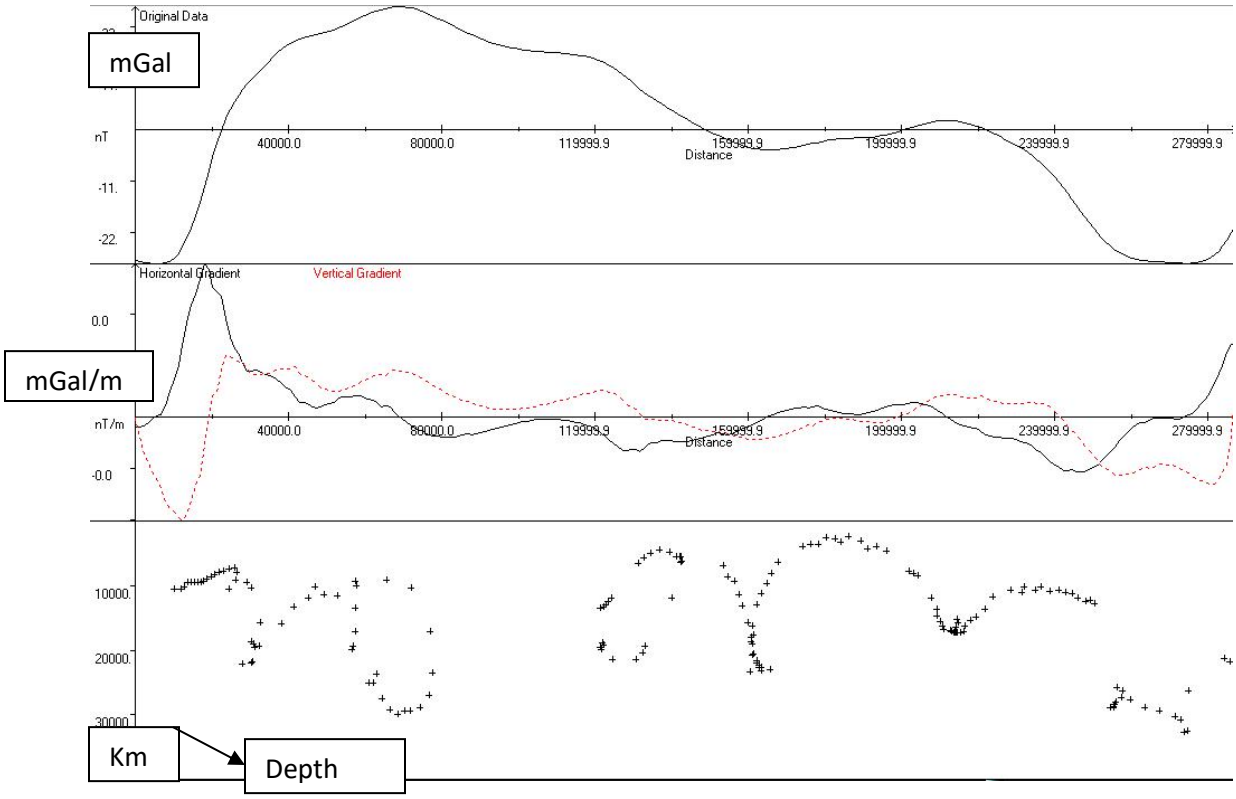

Figure6.10a.Euler deconvolution for profile BB`

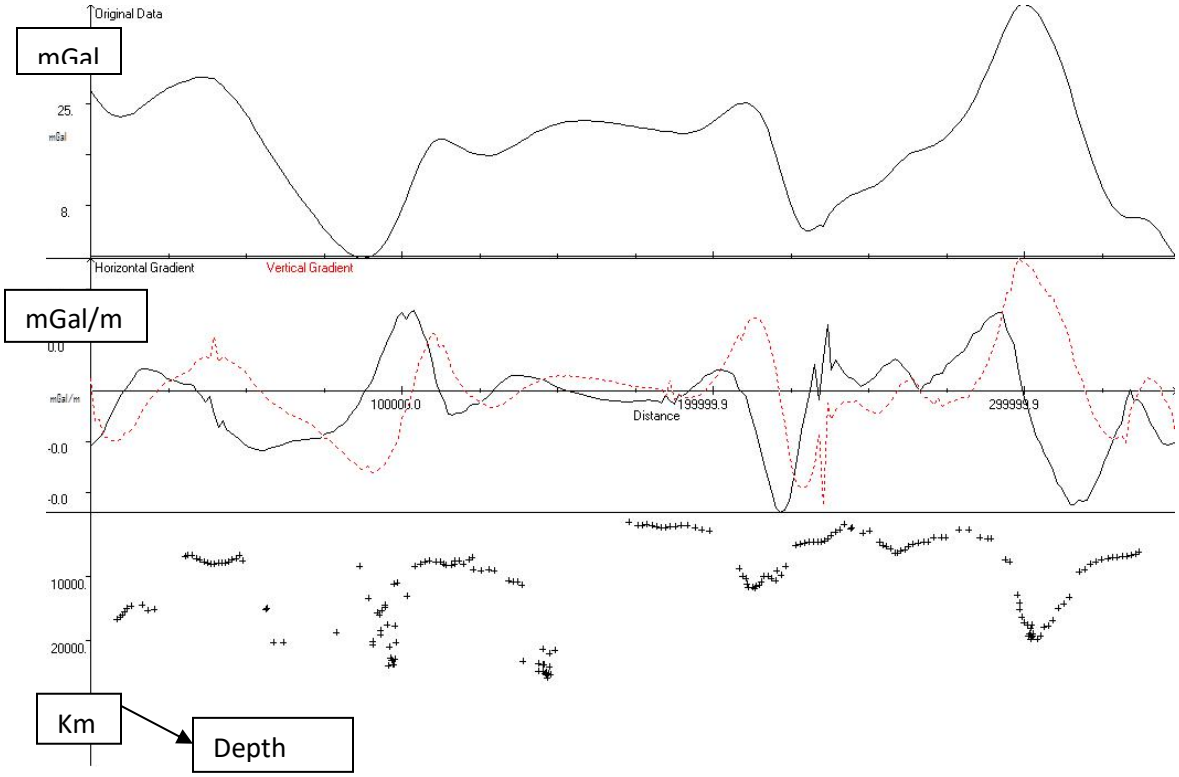

Figure6.10b.Euler deconvolution for profile CC`

CHAPTER SEVEN

GRAVITY MODELING AND INTERPRETATION

Modeling of gravity data could be accomplished by using either the forward modeling technique or inverse modeling technique. Here in this thesis work, forward modeling technique, where an initial structure (model) is prepared using available geological, geophysical and Euler deconvolution results. Once the initial model is prepared, then the gravity anomaly of this model is calculated and compared with the observed anomaly until satisfactory fit is obtained between the calculated and observed anomalies.

7.1. 2.5-D modeling of the Gravity Data

In order to quantify the depth, shape and density of the mass distribution causing the gravity maxima along the selected profiles in the study area, a 2.5 Dimensional (2.5D) gravity model was constructed along and across the main trends of gravity maxima (Figure6.9)

A one-dimensional profile was extracted from the two-dimensional contour maps. Within the two-dimensional contour, two profiles were chosen for modeling purpose (Figure6.9). The profile selection is based on the tendency of the anomaly pattern.

The forward modeling process for the gravity data was conducted with 'Grav2dc' software (Cooper, 2003a, b). The program is based on the Talwani algorithm to calculate anomalies (Talwani et al., 1959).

7.2. Initial Model

To constrain the crustal thickness and density structure, the refraction seismic study in the Afar depression (Makris and Ginzburg, 1987) was used in calibrating crustal thickness and density (Table.7.1). The mean seismic velocities for each layer of the subsurface were converted in to density using the relationship; , where and are constants and their estimated values are 0.252 and 0.3788, respectively (Christensen and Mooney, 1995).

Based on the above velocity density conversion relationship the following initial model is produced.

Rock Type	V_p(km/sec)	(kg/m^3)	Thickness(km)
Unconsolidated sediments and pyroclastic	4.1	2350-2560	3-4
Upper crust	6.1-6.45	2600-2700	7-11
Lower crust	6.6-7.2	2800-2980	15-22
Upper mantle	7.4-7.8	3100-3200	15-19

Table.7.1.Initial model from seismic refraction profile (Makris and Ginzburg, 1987).

Further constraint on depth is obtained from the Euler deconvolution results and from contour map of the Moho depth produced by (Mammo, 2004).

Taking the above initial model as a starting model, initial densities and geometries were varied to get the final models produced for the profiles, BB` and CC` are shown in Figures7.1 (a) and (b) respectively.

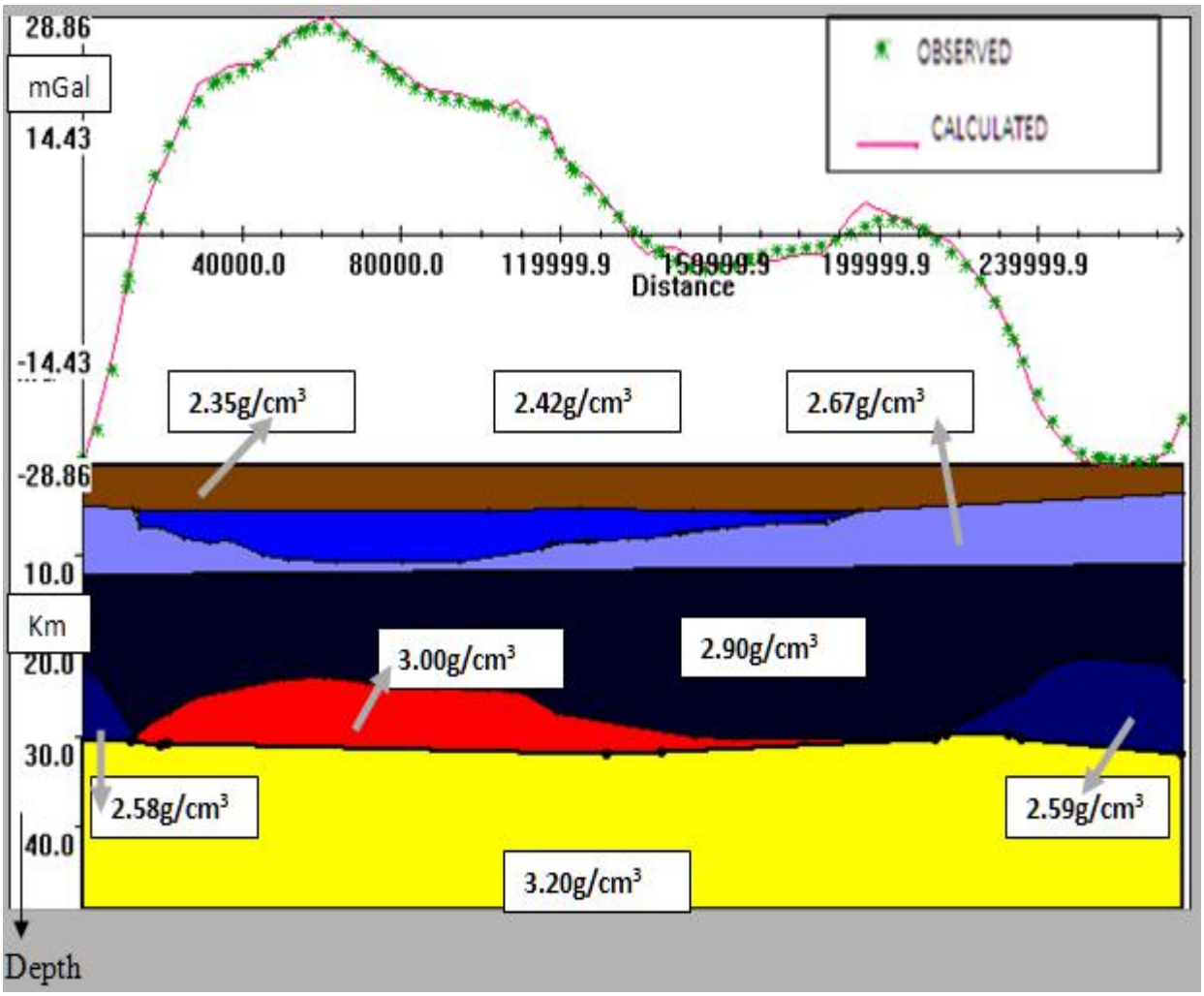

Figure.7.1a.Model along Profile BB`

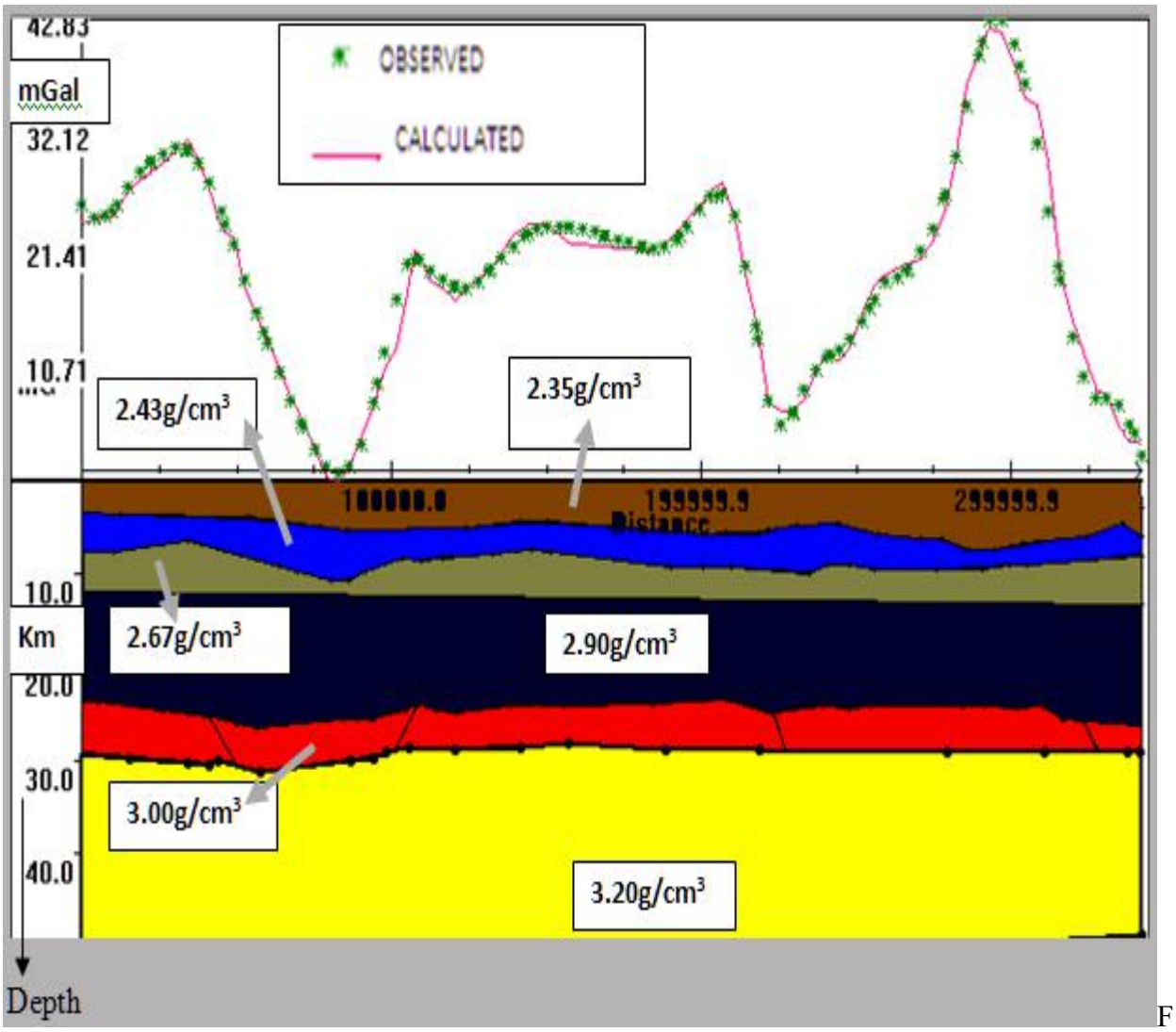

Figure.7.1b.Model along profile CC`

7.3. Interpretation of the Models

7.3.1. Model along profile BB`

This model shows the anomalous mass distribution under profile BB` (striking approximately, EW), which is taken across the main trends of higher residual gravity (Figure6.9).

To model this profile four anomalous bodies are required. One having a density contrast of (–0.25) mGal at (depth to its top) about 4km has a variable thickness with a maximum thickness of about 5km. (-0.25) mGal density contrast corresponds to a density of 2.42gm/cm^3.This low density material could be related to the existence of Mesozoic sediment under the profile considered. Other three anomalous bodies, located at a depth greater than 20km are aligned

horizontally. Two of them are low density materials with density contrasts (-0.095) (bulk density, 2.59g/cm^3) and (-0.085) mGal (bulk density, 2.58g/cm^3) at the eastern and western end of the profile. These low density materials could be attributed to the sialic masses, which may thicken the crust under the plateaus. The middle one with density contrast of 0.3300mGal has a depth to its top 23.5km. A 0.3300mGal density contrast corresponds to a bulk density of about 3.00gm/cm^3. This high density body could be related to a mafic material that may be attributed to an upper mantle material invading the lower crust. Hence, from this model, one can see that the crust thins to 23.5km above this high density material.

7.2.2. Model along Profile CC`

The model along profile CC` shows the possible anomalous mass distribution, which produces the observed gravity along profile CC` (striking nearly NNE - SSW), which is taken along the main trend of higher (positive) residual gravity (Figure6.9). This model consists of a low density material (density contrast of – 0.2400) in the form of a layer with average depth to its top is about 5km. This low density layer has a varying thickness ranging from 2.2km to 5km. A density contrast of (-0.2400) corresponds to a bulk density of about 2.43gm/cm^3, hence this low density layer could again be attributed to the presence of Mesozoic sediment under the profile concerned.

The other high density layer modeled in this profile is located below a depth of 20km. The layer is laterally separated in to 5 blocks by four faults. The faults are also seen in the horizontal gradient calculated together with the Euler deconvolution (Figures.6.10a and 6.10b). These 5 blocks have almost similar densities of 0.3300, 0.3307, 0.3300, 0.3307 and 0.3400 respectively from the SSW end to the NNE end of the profile. The depth to this anomalously higher density layer (taking the separated blocks as one layer) varies from 22.7km at the SSE end to 25.9km at the NNE end of the profile. An average density contrast for this layer is 0.3323mGal. This corresponds to an average bulk density of 3.00gm/cm^3. This layer (high density under plate) could be related to a material of mafic origin corresponding to an upper mantle material, which was also modeled with a wave velocity of 7.4km/sec (Makris and Ginzburg, 1987). According to this model, one can infer that the crustal thickness along this profile varies from 22.7km at the SSE end to 25.9km at the NNE end of the profile.

CHAPTER EIGHT

CONCLUSIONS AND RECOMMENDATIONS

8.1. Conclusions

Analysis and interpretation of the gravity data, obtained from the Ethiopian Institute of Geological survey, was performed qualitatively from the different anomaly maps discussed and quantitatively from the 2.5D forward modeling of the gravity profiles selected across and along the main trends of higher residual gravity.

Generally, from this study one can conclude;

-Relatively higher Bouguer gravity clearly separates the Afar depression from the surrounding (the western Ethiopian plateau, the south east plateau and the opening of Afar to the Main Ethiopian Rift (MER) i.e. southwest apex of the triangular depression). This could be due to the presence of lower density material beneath these areas as compared to the depression. In addition inverse correlation is observed between the Bouguer gravity and the topography.

-The residual anomaly map shows clearly defined trends of higher (positive) gravity values, interpreted to be following the trends of crustal thinning (extension). This elongated anomaly begins at the south west apex of the study region and follows a trend of NE-SW up to about 10^0N and N-S trend where it becomes parallel to the main escarpment. Further north of the study region, it follows NNE-SSW trend whereas (NNW-SSE) and (E-W) in the northwest apex and in the eastern part respectively. This elongated higher (positive) residual value coincides with the trend of crustal thinning (Makris and Ginzburg, 1987).

-Maximum gravity gradient occurred at the southwest apex and south of the study region, which may be related to faulted structures. N-S trending relatively higher gradient, which coincides with the western boundary of Afar, may be attributed to the bordering escarpments while the other relatively higher gravity gradient (trending in ENE-WSW) coincides with the boundary of Afar and southeastern plateau, which could also be attributed to south eastern escarpment. High gradients in the central and north western

part of the study area may be attributed to localized structures (probably graben structures).

-Generally speaking, strong regional anomaly is observed in the study area. The maximum and minimum regional values are observed at the northeast End and southeast End of the study region. Even though, relatively higher regional values are observed in the Afar depression, still the values are negative. The regional absence of a strong positive regional values agrees with the Wegner`s (1929) observation that the elevation of most of Afar above sea level points to the presence of sialic masses beneath the lava cover. There is an inverse relation between the topographic relief and regional gravity field in the study region. This is associated with isostatic compensation of the topographic relief by low density material at depth (Makris et al., 1975).

-Based on the modeling results on both profiles a low density material (interpreted to be Mesozoic sediment) with a maximum thickness of about 5km is found at (depth to top) at 4km and 5km below profiles BB` and CC` respectively. A high density material (which could be an upper mantle material) was found at (depth to top) 23.5km and 22.7km, which causes the crustal extension. This result shows a crustal thickness of about 23.5km and 22.7km under profile BB` and CC` respectively.

-Four deep seated faults were also revealed under profile CC`.

8.2. Recommendations

Based on the study the following recommendations are forwarded:

-Due to the ambiguity problems inherent in gravity method other geophysical methods such as seismic should be done to justify the results.

-The modeling result shows that a significant thickness of Mesozoic sediment, having a maximum thickness of about 5km. This could be considered as a potential target for petroleum exploration.

-Thinner crust and deeper faults tells us that there need to be a continuous follow up to understand the tectonic activities that may affect the area.

REFERENCES

Almond, D.C.(1986) Geological evolution of the Afro-Arabian dome. *Tectonophysics* 331:302–333.

Barberi, F., Varet, J.(1977) Volcanism of Afar: small-scale plate tectonics implication. *Geological Society of America Bulletin* 88:1251–1266.

Barberi, F., Borsi, S., Ferrarea, G., Marinelli, G., Santcroce, R. Tazief, H., Varet, J.(1972) Evolution of the Danakil Depression (Afar Ethiopia) in light of radiometric age determination. *Journal of Geology* 80: 720–729.

Barberi, F., Bonati, E., Marinelli, G., Varet, J.(1974) Transverse tectonic during the split of continent: Data from the Afar rift. *Tectonophysics* 23:17–19.

Bergzabren, Germany.(1974) vol. **1**. E: Schweizerbart sche Verlagsbuchhandlung, Stuttgart, Germany, pp. 174–178.

Berhe, S.M., Desta, B., Nicoletti, M., Teferra, M.(1987) Geology, geochronology and geodynamic implications of Cenozoic magmatic province in W and SE Ethiopia. *Journal of the Geological Society of London* 144: 213–226.

Beyene and Abdelsalam (2005) Tectonics of the Afar Depression: A review and synthesis. *Journal of African Earth Sciences* 41**:** 41–59

Black, R., Morton, W.H., Hailu, T.(1974) Early structure around the Afar triple junction. *Nature* 248: 496–497.

Bosworth, W., McClay, K.(2001) Structural and stratigraphic evolution of the Gulf of Suez Rift, Egypt: a synthesis. *Memoires due Museum National dltistorire nationalle* 186: 567–606.
Fuchs, K., Altherr, R., Mueller, B., Prodehl, C. (Eds.)Structure and Dynamic Processes in the Lithosphere of the Afro-Arabian Rift System. *Tectonophysics* 278: 47–62

Cordell, L.(1979) Gravimetric expression of graben faulting in Santa Fe Country and the Espanola Basin, New Mexico: New Mexico. Geol. Sot. Guidebook, 30th Field Conf., pp. 59-64.

Collet, B., Taud, H., Parrot, J.F., Bonavia, F., Chorowicz, J.(2000) A new kinematic approachfor the Danakil Block using a digital elevation model representation. *Tectonophysics* 316: 343–357.

Cooper, G.R.J.(2003a). Grav2dc, V.2.10 for Microsoft windows. School of Geosciences University of the Witwatersrand, Johannesburg, South Africa [Online]. [Accessed 19thMay 2009]. www.cooperg@geosciences.witz.ac.za

Courtillot, V.E.(1980) Opening of the Gulf of Aden and Afar by progressive tearing. *Physics of the Earth and Planetary Interiors* 21: 343–350.

Courtillot, V.(1982) Propagating rifts and continental breakup. *Tectonphysics* 1: 239–250.

Courtillot, V., Achache, J., Landre, F., Bonhommet, N., Montigny, R., Feraud, G.(1984) Episodic spreading and rift propagation; new paleomagnetic and geochronologic data from the Afar nascent passive margin. *Journal of Geophysical Research* 89: 3315–3333.

Courtillot, V., Armijo, R., Tapponnier, P.(1987) Kinematics of the Sinai triple junction and a two phase model of Arabia–Africa rifting continental extensional tectonics. *Geological Society Special Publications* 28:559–573.

CNR-CNRS-Afar team. (1973) Geology of northern Afar (Ethiopia).*Revue de Geographie Pysique et de Geologie Dynamique* 2: 343–390.

DOBRIN, M.B., AND SAVIT, C.H.(1988) Introduction to Geophysical Prospecting. McGraw – Hill Inc. Singapore p. 630.

Ebinger, C.J., Casey, M.(2001) Continental breakup in magmatic provinces: an Ethiopian example. *Geology* 29: 527–530.

Ebinger, C.J., Sleep, N.H.(1998) Cenozoic magmatism throughout East Africa resulting from impact of a single plume. *Nature* 395: 788–791.

Ebinger, C.J., Yemane, T., WoldeGabriel, G., Aronson, J.L., Walter, R.C.(1993) Late eocene-recent volcanism and faulting in the southern Main Ethiopian Rift. *Journal of the Geological Society of London* 150: 99–108.

Ghebreab, W.(1998) Tectonics of the Red Sea region reassessed. *Earth Science Reviews* **45**, 1–44.

Ghebreab, W., Carter, A., Hurford, A.J., Talbot, C.J.(2002) Constraints for timing of extensional tectonics in the western margin of the Red Sea in Eritrea. *Earth and Planetary Science Letters* 200: 107–119.

Hofmann, C., Courtillot, V., Feraud, G., Rouchett, P., Yirgu, G., Ketefo, E., Pik, R.(1997) Timing of the Ethiopian flood basalt. *Tectonophysics* 141: 199-214.

Kazmin, V.G., Byakov, A.F.(2000) Magmatism and crustal accretion in continental rifts. *Journal of African Earth Sciences* 30: 555–568.

Makris, J., Ginzberg, A.(1987): The Afar depression: transition between continental rifting and sea-floor spreading. *Tectonophysics* 141: 199–214.

Mammo, T.(2004) Mapping the crust-mantle boundary beneath Afar depression. *Gondwana Research* 7: 855–861.

McKenzie, D.P., Davis, D., Molnar, P.(1970) Plate tectonics of the Red Sea and East Africa. *Nature* 226: 243–248.

Mickus .K[a,*], Ketsela Tadesse [b], G.R. Keller [b], Befekadu Oluma [c] (2007)Gravity analysis of the main Ethiopian rift. *Journal of African Earth Sciences* 48**:** 59–69

Mickus, K. L., and Peeples, W. J.(1992) Inversion of gravity and magnetic data for the lower surface of a 2.5 dimensional sedimentary basin: Geophysical Prospecting, 40, pp. 171-194.

Mohr, P.A.(1975) Structural setting and evolution of Afar. In: Pilger, A., Rosler, A. (Eds.), Afar Depression of Ethiopia, Proceedings of an International Symposium on the Afar Region and Rift Related Problems, Bad Bergzabren, Germany, 1974, vol. 1. E. Schweizerbart_scheVerlagsbuchhandlung, Stuttgart, Germany, pp. 27–37.

Montenat, C., Ott d_Estevou, P., Purser, B.H. (1998) The Suez Rift and the north-western Red Sea Neogene sedimentation and tectonic evolution. In: Purser, B.H. (Ed.), Dynamics and Methods of Study of Sedimentary. Oxford and IBH Publishing Company, New Delhi, India, pp. 173–199.

Moritz, H., 1984: Geodetic Reference System (1980) In: C.C. Tscherning (ed), The Geodesist's Handbook 1984: *Bull Geod*. 58: 388-398

Pallister, J.S.(1987) Magmatic history of Red Sea rifting; perspective from the central Saudi-Arabian coastal plain. *Geological Society of America Bulletin* 98: 400–417.

Purcell, P.G.(1976) The Marda Fault Zone, Ethiopia. *Nature* 261: 569–571.

Sultan, M., Becker, R., Arvidson, R.E., Shore, P., Stern, R.J., El Alfy, Z., Guinness, E.A.(1992) Nature of the Red Sea crust: a controversy revisited. *Geology* 20**:** 593–596.

Talwani, M, Worzel, JL, and Landisman, M.(1959) Rapid Gravity Computations for Two-Dimensional Bodies with Application to the Mendocino Submarine Fracture Zone,

Journal of Geophysical Research, 64**:** 49-61.

Tefera, M., Chernet, T., Haro, W.(1996) Explanation of the Geological Map of Ethiopia. Ethiopian Institute of Geological Surveys, Addis Ababa, vol. 3, p. 79. Vail, J.R., 1985. Pan-African (late Precambrian) tectonic terrains and reconstruction of the Arabian–Nubian Shield. *Geology* 13: 839-842.

Telford, W.M., Geldart, L.P., and Sheriff, R.E.(1990) Applied Geophysics, Cambridge Univ. Press p.860.

Tessema.A*,L.A.G. Antoine (2004) Processing and interpretation of the gravity field of the east African Rift: implication for crustal extension. *Tectonophysics* 394: 87-110

Tiberi, C., Ebinger, C., Ballu, V., Stuart, G., Oluma, B.(2005) Inverse models of gravity data from the Red Sea-Aden-East African rifts triple junction zone. *Geophysical Journal International* 163: 775–787.

Varet, J.(1978) Geology of Central and Southern Afar (Ethiopia and Djibouti Republic) F. Gasse for Chapter IV on Sedimentary Formation. Eds. CNRS, France, Paris, p. 118.

Vellutini, P.(1990) The Manda-Inakir Rift, Republic of Djibouti: A comparison with the Asal Rift and its geodynamic interpretation. *Tectonophysics* 172: 141–153.

White, R., McKenzie, D.(1989) Magmatism at rift zones; the generation of volcanic continental margins and flood basalts. *Journal of Geophysical Research* 94: 7685–7729.

DECLARATION AND COPYRIGHT

I declare that this thesis is my original work and has not been prepared for any degree in any university, and that all the sources of materials used for the thesis have been duly acknowledged.

Name: Dessalegn Tekle Signature _____ Date _____

This thesis has been submitted for examination with my approval as University advisor.

Dr. Tilahun Mammo		
Advisor	Signature	Date